Isolation and partial characterization of three acetylcholine-gated chloride channels in *Haemonchus contortus*

by

Micah Callanan

A Thesis Submitted in Partial Fulfillment
of the Requirements for the Degree of

Master of Science

in

Applied Bioscience

University of Ontario Institute of Technology

ABSTRACT

Haemonchus contortus is a parasitic nematode infecting ruminants causing anemia and poor health due to the parasite's blood-feeding nature. The ability to manage infection has been confounded by the rapid development of antiparasitc drug resistance in *H. contortus* populations. The Cys-loop superfamily of ligand gated ion channels are well recognized as critical drug targets for many invertebrate specific compounds. With the rise in resistance seen worldwide to existing anthelmintics, novel drug targets must be identified so new treatments can be developed. This thesis describes the identification of three acetylcholine-gated chloride channelss (*hco-acc-1, hco-acc-2, and hco-acc-4)* genes from the nematode parasite *Haemonchus contortus* and provides evidence suggesting that they could be developed as a future anthelmintic targets. While these genes appear similar in sequence to the previously characterized *C. elegans acc-1*, *acc-2* and *acc-4* genes, Hco-ACC-2 is about 2-fold less sensitive to acetylcholine, perhaps indicating a different *in vivo* function within the parasite. Further pharmacological analysis of ACC-2 via two-electrode voltage-clamp electrophysiology demonstrated activity of several agonists including carbachol, which elicited a similar response as acetylcholine. Furthermore, *in silico* protein modelling and agonist docking of all three channels has revealed a unique agonist binding site with several novel residues that appear to be important for binding to cholinergic agonists. Antibodies were generated against the Hco-ACC-1 protein for use in immunolocaliztion studies. Hco-ACC-1 localizes to the anterior half of the pharynx, specifically in pharyngeal muscle tissue in *H. contortus*.

CERTIFICATE OF APPROVAL

TABLE OF CONTENTS

ABSTRACT…… II

CERTIFICATE OF APPROVAL…….. III

LIST OF FIGURES……... VI

LIST OF TABLES……..... VII

LIST OF ABBREVIATIONS AND SYMBOLS…… VIII

ACKNOWLEDGEMENTS…….. IX

CHAPTER 1: INTRODUCTION AND LITERATURE REVIEW 1

SECTION 1.1: INTRODUCTION…… 1

SECTION 1.2: BACKGROUND…… 1

SECTION 1.2.1: H*AEMONCHUS CONTORTUS*…… 1

SECTION 1.2.2: LARVAL (FREE-LIVING) LIFE-STAGE…… 2

SECTION 1.2.3: PARASITIC ADULT LIFE-STAGE…… 3

SECTION 1.2.4: LARVAL TO ADULT LIFE-STAGE TRANSITION…… 3

SECTION 1.2.5: THE NEMATODE PHARNYX…… 3

SECTION 1.3: LIGAND-GATED ION CHANNELS (LGICS)…….. 7

SECTION 1.3.1: STRUCTURE…… 7

SECTION 1.3.2: NEMATODE LGICS……... 10

SECTION 1.3.3: THE ACETYLCHOLINE-GATED CHLORIDE CHANNELS (ACCS)…… 11

SECTION 1.3.4: THE BINDING SITE OF LGICS…….. 14

SECTION 1.3.5: RATIONALE AND OBJECTIVES OF THE RESEARCH…….. 18

CHAPTER 2: METHODS 19

SECTION 2.1: RNA ISOLATION AND CDNA PRODUCTION…… 19

SECTION 2.2: SEMI-QUANTITATIVE PCR AND DENSITOMETRY…… 19

SECTION 2.3: ISOLATION OF *HCO-ACC-1*, *HCO-ACC-2*, *HCO-ACC-4*…… 20

SECTION 2.4: EXPRESSION OF ACC-2 IN *X. LAEVIS* OOCYTES……..…….. 20

SECTION 2.5: ELECTROPHYSIOLOGICAL RECORDINGS……..... 22

SECTION 2.6 *IN-SILICO* HOMOLOGY PROTEIN MODELLING……..…….. 23

SECTION 2.7: *COMPUTATIONAL* AGONIST DOCKING……..……. 24

SECTION 2.8: IMMUNOLOCALIZATION OF ACC-1 IN *H. CONTORTUS*……..…….. 24

CHAPTER 3: RESULTS 26

SECTION 3.1: ISOLATION AND CHARACTERIZATION OF *HCO-ACC-1*, *HCO-ACC-2*, *HCO-ACC-4*… 28

SECTION 3.2: IMMUNOLOCALIZATION OF HCO-ACC-1 IN *H.CONTORTUS*…….. 35

SECTION 3.3: ELECTROPHYSIOLOGY…… 37

SECTION 3.4: *IN-SILICO* HOMOLOGY PROTEIN MODELLING…… 39

CHAPTER 4: DISCUSSION AND CONCLUSION 44

SECTION 4.1: CHARACTERIZATION OF HCO-ACC-1 …… 44

SECTION 4.2: CHARACTERIZATION OF HCO-ACC-2 …… 46

SECTION 4.3: CHARACTERIZATION OF HCO-ACC-4…… 47

SECTION 4.4: OTHER POTENTIALLY IMPORTANT RESIDUES IN ACC-1, 2 AND 4 …… 48

SECTION 4.5: CONCLUSION …… …….. 50

REFERENCES 51

LIST OF FIGURES

Figure 1.1 – The *Haemonchus contortus* life-cycle…….. 2

Figure 1.2 – Three nematode pharyngeal configurations …….. 6

Figure 1.3 – The *C. elegans* GluCl crystal structure (PDB, 3RIA)…….. 8

Figure 1.4 – 3RIA dimer illustrating a single functional agonist binding site…… 9

Figure 1.5 – Two subunits of 3RIA with the six major binding loops highlighted…… 15

Figure 1.6 – Hco-ACC-2 homology model with acetylcholine docked…..…….…. 16

Figure 3.1 – Initial end-point PCR amplification and densitometry……..... 27

Figure 3.2 – Clustal Omega multiple sequence alignment of Hco-ACC-1,2, and 4..... 29

Figure 3.3 – Homology model of Hco-ACC-1 based on 3RIA…….…….. 30

Figure 3.4 – Amino acid sequence alignment of Hco-ACC-1 and Cel-ACC-1……..30

Figure 3.5 – Homology model of Hco-ACC-2 based on 3RIA…….……32

Figure 3.6 – Amino acid sequence alignment of Hco-ACC-2 and Cel-ACC-2……..32

Figure 3.7 – Homology model of Hco-ACC-4 based on 3RIA……. 34

Figure 3.8 – Amino acid sequence alignment of Hco-ACC-4 and Cel-ACC-4…….. 34

Figure 3.9 – Representative electrophysiological tracings of Hco-ACC-2 receptors in response to a variety of agonists and percent of max ACh response ……. 36

Figure 3.10 – Dose response curve of Hco-ACC-2 (n=6) to increasing concentrations of acetylcholine…….. 37

Figure 3.11 – Immunolocalization of Hco-ACC-1 in MOF23 and PF23 adult female *H. contortus* worms …….. 38

Figure 3.12 – Potential agonist binding site configurations of ACC-1, ACC-2, ACC-4... 41

Figure 3.13 – Different agonists docked to the Hco-ACC-2 homodimer……..…….…. 42

LIST OF TABLES

Table 1 – Calculated affinities and distances of ACh to the binding site of the modelled Hco-ACC-1, Hco-ACC-2, and Hco-ACC-4……43

Table 2 – Calculated affinities and distances of ACh, carbachol, and urecholine to the binding site of the Hco-ACC-2 homology modelled dimer…… 43

LIST OF ABBREVIATIONS AND SYMBOLS

5-HT: 5-Hydroxytryptamine (Serotonin)

ACC: (Nematode) Acetylcholine-Gated Chloride (Channel)

ACh: Acetylcholine

Asn(N): Asparagine

A. suum: *Ascaris suum*

Carbachol: Carbamylcholine

C. elegans (Cel): *Caenorhabditis elegans*

Cys(C): Cysteine

ECD: Extracellular Domain

FAB: Antigen binding fragment of the antibody used to crystallize 3RIA.

GABA: γ-aminobutyric acid

GFP/YFP: Green/Yellow fluorescent protein

GGR: Subunit notation for some genes of the GABA/Glycine Receptor family.

GluCl: Glutamate-gated Chloride (Channel)

GlyR: Glycine Receptor

H. contortus (Hco): *Haemonchus contortus*

IVM: Ivermectin

LGIC: Ligand-Gated Ion Channel

LGC: Ligand-gated channel (gene/protein notation)

nAChR: Nicotinic Acetylcholine

Phe(F): Phenylalanine

M (#): Transmembrane domain (1-4)

Trp (W): Tryptophan

Tyr (Y): Tyrosine

UNC: Protein name based on an uncoordinated phenotype observed in organisms when knocked out.

X. laevis: *Xenopus laevis* (African clawed frog)

ACKNOWLEDGEMENTS

I am grateful for the opportunity that was afforded me by the University of Ontario Institute of Technology (UOIT) to explore the many facets of Biology in such a unique way. All the instructors who have guided me in my path through post-secondary education truly had a greatly positive impact on my life.

Foremost, I wish to thank Dr. Sean Forrester, my supervisor during my graduate studies. I am sure many graduate students believe they have great supervisors, but I feel Sean would be amongst the very best. I very much appreciate all the guidance, patience, and expertise you imparted on me. Beyond that, I am truly grateful for how you always encouraged original thought, and to examine anything I felt was interesting which always allowed me to develop problem solving skills and think for myself. Additionally, your guidance and support through some difficult times always steered me in the right direction, which I believe far exceeded what anyone would reasonably expect from a supervisor. You always went above and beyond for me, something I will never forget.

To the countless graduate (and undergraduate students) I encountered throughout my studies at UOIT, I thank you all. I learned so many things and had some great conversations with you folks (always outside Dr. Bonetta's lab, wherever that may have been found). Special thanks to Mark Kaji, we started at the same time, and my journey was always shaped very positively by you. The effort you put into figuring out electrophysiology and then teaching it to me was an amazing feat, the Forrester lab may have been in serious trouble had you not put in the inhuman effort in those 2 years.

Derek Tilley and Sarah Warren, I really enjoyed my time when you guys were around, Derek for teaching me probably the most important single life lesson I have ever learned, and now shapes my entire outlook, and Sarah being the most supportive work mother a guy could have. My scheduling ability took a huge hit when you left. Isaac Shim, thanks for all those coffee chats about countless topics. Justin McCarville, miss our chats, and hearing you slam those ELISA's. Josh Foster, it was great having you in the lab, the music selection was ever diversified with you there, Oh, hi Doggy! Everett Cochrane, you were also great to have in the lab, especially for that brief period with Siddiq "hunting" on campus, with our phones and also for that last-minute prism save.

To all my undergrad students, each of you had a great impact on me, I can only hope I helped each of you in your journeys in some way. Sara, thanks for all the quick chats on breaks, always interesting, hope the PhD goes well. A special thank you to McGill University for hosting me for a summer of study, what a great experience. To all those at McGill University (especially Dr. Robin Beech, and Dr. Thomas Duguet) for teaching me so many new things, and allowing me to complete some interesting research.

Lastly, but certainly most importantly, I would like to thank my family. Mom and Dad, your eternal patience and understanding is something that everyone in the world should strive for. The encouragement and love I have received in my life from you two cannot be described in words, I will always be eternally thankful, and I hope I can make you as proud as I am to have such great parents. Natalie and Roxy, the two most beautiful ladies I have ever seen, thank you for everything you have done for me. There are no words I could put here that could ever do any justice to the way I feel about you, or how thankful I am for you. This thesis is dedicated to you.

CHAPTER 1: INTRODUCTION AND LITERATURE REVIEW

1.1 Introduction

Haemonchus contortus is a blood-sucking parasitic worm of the abomasum which mainly infects ruminants such as cattle, sheep and goats. Parasitic nematodes such as *H. contortus* are controlled through the use of broad spectrum nematocidal chemotherapeutics such as ivermectin (IVM) and newer drugs such as monepantel (Kaminsky *et al.* 2008). Drugs such as these disrupt the nervous system of nematodes by interacting with ligand gated ion channels. However, *H. contortus* and several other parasitic nematodes have shown the ability to become resistant to multiple anthelmintic drugs including ivermectin, levamisole, and moxidectin (Saeed *et al.* 2010, Tyrell and LeJambre, 2010, Almeida *et al.* 2010). The emergence of anthelmintic resistance in *H. contortus* has made the search for the next generation of anti-parasitic drug targets vital. Indeed, the discovery and characterization of new types of ligand-gated ion channels with unique binding and activation mechanisms may lead to discovery of new types of effective anthelmintics.

1.2 Background

1.2.1 Haemonchus contortus

H. contortus, also known as the barber pole worm, is an organism of great economic importance due to its ability to cause severe illness and death of cattle and other ruminants which is detrimental to the agriculture industry worldwide. *H. contortus* belongs to the phylum *Nematoda* and more specifically to the super family *Trichostrongyloidae* (GenBank: Taxonomy ID 6289).

While the parasite has origins in Africa, it is also a current agricultural burden in North America (Hoberg *et al.* 2004). *H. contortus,* first described in 1915 by Veglia, exists in two major life-stages; the free living larval stage and the parasitic adult stage which is reviewed in Figure 1.1.

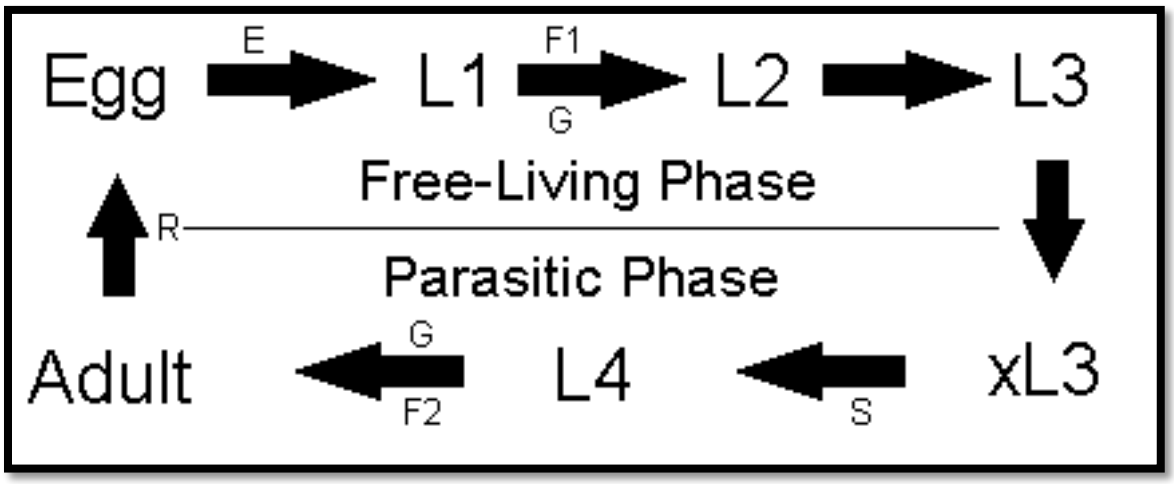

Figure 1.1 - The *Haemonchus contortus* life-cycle adapted from Nikolaou and Gasser, 2006. **(E)** Embryogenesis, **(S)** Sexual differentiation, **(R)** Reproduction, **(F1)** Bacterial-feeding phase, **(F2)** Blood-feeding phase, **(G)** Rapid growth phase, **(xL3)** exsheathed.

1.2.2 Larval (free living) life-stage

H. contortus has 4 larval stages (L1-L4) each broken up into 2 phases. The first phase is characterized as growth and feeding stage, the second being a stage of morphological change known as lethargis (Nikolaou and Gasser, 2006). Larvae will emerge as the next stage immediately after the previous stage has completed lethargis, in a newly synthesized cuticle. When the L3 larvae are consumed from the environment by a suitable host, they will sexually differentiate and begin blood feeding, followed by maturation into the adult stage.

1.2.3 Parasitic adult life-stage

After maturation, the adult male and female parasites will continue feeding on blood and copulate. Female parasites will begin laying eggs approximately 18 days after oral ingestion of the parasite by the host (Nikolaou and Gasser, 2006). A female parasite can lay up to 4500 eggs per day (Coyne and Smith, 1992) and can grow to be 30mm in size (Nikolaou and Gasser, 2006). Eggs are laid at the 4-cell stage and released into the environment in the fecal matter of the host at the 11-26 cell stage, as oxygen is required for further development (Nikolaou and Gasser, 2006).

1.2.4 Larval to adult life-stage transition

The transition of *H. contortus* from free living to parasitic life-stage is stimulated by CO_2 and controlled by the enzyme carbonic anhydrase. This enzyme releases noradrenaline which causes the activation of a number of genes responsible for the exsheathing of fluid responsible for L2 moulting (shedding of cuticle) (Nikolaou and Gasser, 2006). It appears that CO_2 chemosensory neurons of the amphids (sensory organs) (Ashton *et al.* 1999) are responsible for this change. However, this mechanism is poorly understood.

1.2.5 The nematode pharynx

The nematode pharynx is a muscular organ that is able to contract rhythmically to send food to the intestines. There is significant divergence in the structure of the pharynx between nematodes. The *A. suum* (a parasite of pigs) pharynx is a muscular organ comprised of a tri-radiate lumen. The interior of the pharynx is lined with cells derived from the cuticle.

The muscle surrounding the pharynx is analogous to vertebrate smooth muscle. Pharyngeal pumping is mediated by externally radiating muscle tissue that is located between the internal and external surfaces of the pharynx (Stretton *et al.* 1992). The assembly is similar to vertebrate diaphragm muscle, such that, contractions actually increase the size of the lumen (decreasing the intra luminal pressure), enabling suction. Relaxation decreases the size of the lumen, increasing intra luminal pressure, pushing contents posteriorly down into the intestines (Harris, 1957). The *A. suum* pharynx shows no distinct bulbs as seen in the model nematode *C. elegans*. Contractions in the pharynx of *A. suum* start at the most anterior point and travel posteriorly to the valve located at the anterior end of the intestines (posterior end of the pharynx) (Reger, 1966). The anterior tip of *A. suum* initiates contraction either through myogenic contraction or by enteric nervous system activity (Reger, 1966).

In contrast, the *C. elegans* pharynx is bilobed, with the anterior lobe (metacorpus) preceded anteriorly by the procorpus joined to a posterior lobe (terminal bulb) by the isthmus (Albertson and Thomas, 1976). The isthmus is enclosed by the nerve ring responsible for the rhythmic contractions involved with the swallowing and delivery of bacteria to the intestines (Albertson and Thomas, 1976). Bacteria are first ingested into the buccal cavity via contraction (and widening of the pharyngeal lumen), and passed via rhythmic contractions through the remaining 5 components of the pharynx (moving anteriorly); procorpus, metacorpus, isthmus, terminal bulb and finally the pharyngeal intestinal valve (Albertson and Thomas, 1976).

The terminal bulb contains a grinder responsible for mechanically breaking down the ingested bacteria. In total, the *C. elegans* pharynx is comprised of 77 cells, most notably, 34 muscle cells and 20 neuronal cells that make up the pharyngeal nervous system. The 20 nervous cells exist as paired and non-paired neurons (unbranched) (Albertson and Thomas, 1976). These neurons are found between the hypodermis (of the basement membrane) and pharyngeal muscle. Single neuronal processes can actually have both pre and post-synaptic compartments. This means that these neurons do not have axons and dendrites *per se* (Albertson and Thomas, 1976).

Structurally the *C. elegans* pharynx has two large clearly distinct lobes and operates via coordinated contractions. *A. suum* appears to have no distinct lobes, and operates via peristalsis. The structure of the *H. contortus* pharynx has been particularly neglected; however, it appears to lie 'between' the model organism *C. elegans*, and the parasitic nematode *A. suum* in terms of shape/physiology. There are no distinct lobes, but the adult parasite does have a visible pseudo-lobe located in the anterior half of the pharynx. This pseudo-lobe does appear, by inspection, to make *H. contortus* divergent from *A. suum* in terms of pharyngeal anatomy (see Figure 2.6 B and D). It has been shown that many parasitic nematodes essentially have two distinct pharyngeal configurations, one of each present in larval life-stages, the other exclusively present during the adult (or parasitic) life-stage. *H. contortus* appears to have what is known as a filariform pharynx during the adult (blood feeding, life-stage).

This type of pharynx is generally present in parasites of the Trichostrongylidae family and is simply characterized as a one part pharynx, uniformly cylindrical and narrow.

This is in contrast to the strongyliform pharynx (*A. suum)* which is considered a two-part pharynx (Figure 1.2). The strongyliform pharynx is comprised of a corpus which may or may not be separated from a procorpus by an isthmus (Davis *et al.* 1992). The procorpus (anterior) can additionally have wider (swollen) muscle tissue compared to tissues found in the corpus (posterior, towards the gut) (Figure 1.2). Lastly, *C. elegans* has what is known as a rhabditiform or three-part pharynx (Figure 1.2). This form of the pharynx seems to be present in many nematodes, including larval life-stages of parasites. This three-part pharynx has clearly defined regions around two functional bulbs, with anterior bulb being referred to as the metacorpus (White *et al.* 1988).

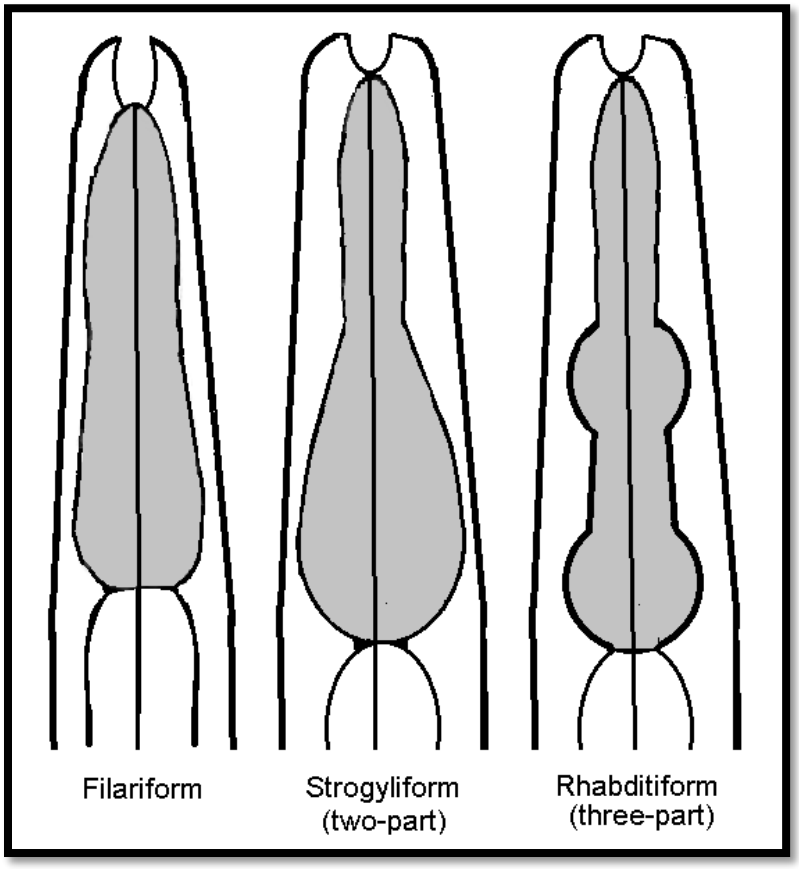

Figure 1.2 – A cartoon representation of 3 variations of the nematode pharynx. The pharynx itself in each instance is coloured gray, and is in contact posteriorly with the intestines of the respective organisms (adapted from Chitwood *et al.* 1950).

1.3 Ligand gated ion channels (LGICs)

1.3.1 Structure

LGICs represent a class of transmembrane spanning proteins responsible for the conductance of ions and subsequent changes in membrane potential. These channels can vary in the structure of their binding sites which bind agonists and antagonists, as well as the type of ions that can cross the channel pore. Despite the fact that these channels do share common characteristics, the overall function of the channels can be highly variable. LGIC's are responsible for both excitatory and inhibitory synaptic transmission in vertebrates and invertebrates. In vertebrate organisms, excitatory receptors are mainly regulated by the neurotransmitters serotonin and acetylcholine (Sine and Engel, 2006). On the other hand, inhibitory receptors are generally regulated by γ-aminobutyric acid (GABA) or glycine (Rajendra *et al.* 1995). When activated, excitatory signals are propagated through the activation of cationic ion channels which will conduct positive ions (such as sodium) from the extracellular region to the interior of a neuron, depolarizing the membrane leading to action potential (Krnjevic, 1974). Conversely, inhibitory signals are propagated through the activation of an anionic channel, conducting negative ions (such as chloride) into the cell hyperpolarizing the neuron leading to a decreased probability of an action potential being formed (Krnjevic, 1974).

Structurally, LGICs in both vertebrates and invertebrates are composed of either a homomeric (5 identical subunits) or, more commonly, a heteromeric (5 non-identical subunits) pentamer (see Figure 1.3). Each subunit, in turn, is composed of four transmembrane domains (M1 – M4) (Figure 1.4), as well as an N-terminus region which contains the agonist binding site (Figure 1.4 and 1.5) responsible for the activation of the channel (Rajendra *et al.* 1995).

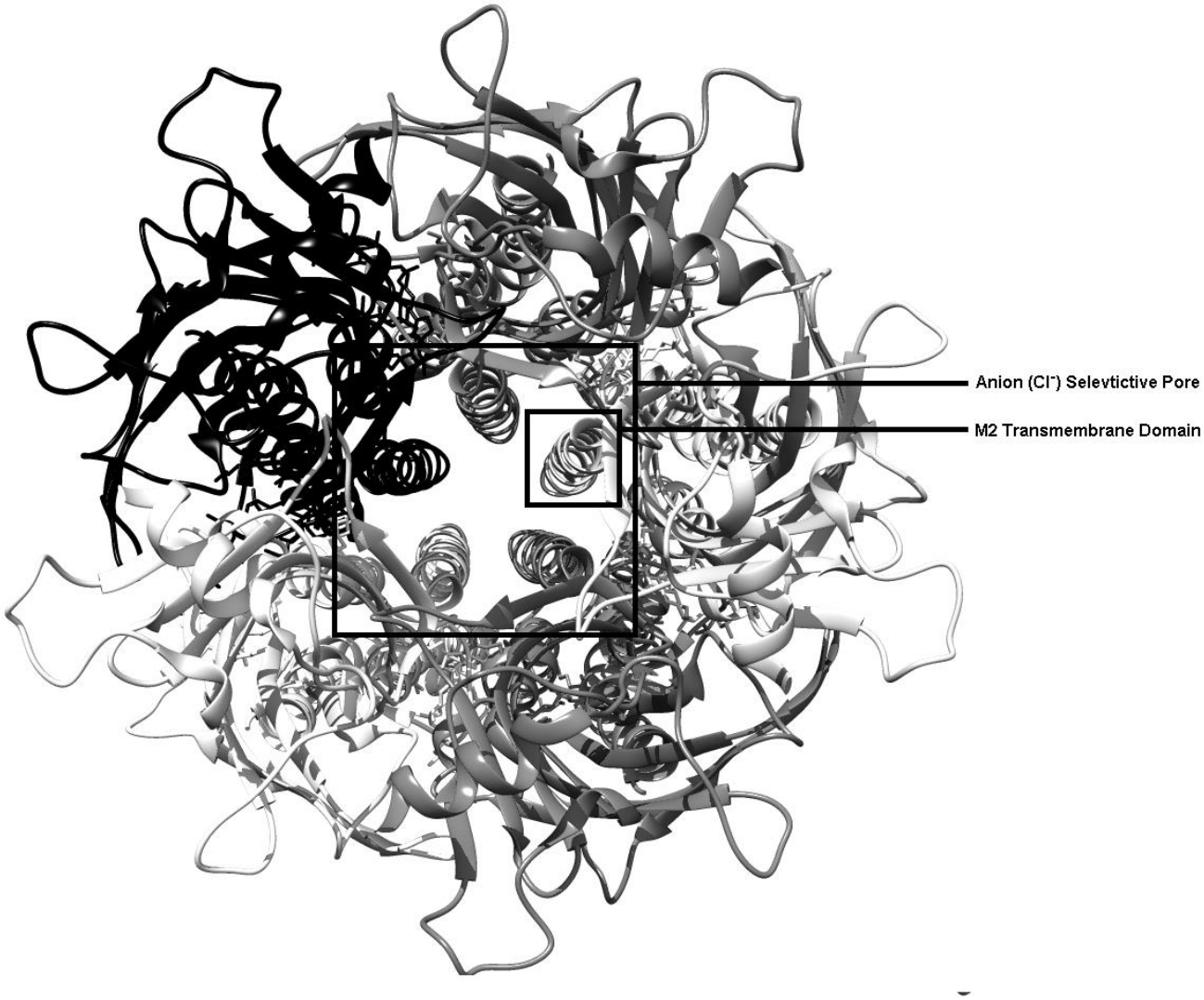

Figure 1.3 - Computer generated image illustrating the crystal structure of the *C. elegans* glutamate gated chloride channel in complex with the antigen binding fragment (FAB), ivermectin (IVM), and iodide (PDB: 3RIA). The view is through the channel pore with the extracellular portion of the pentamer in front. A single subunit's M2 transmembrane domain is highlighted to show how this domain is responsible for the gating mechanism seen in LGICs.

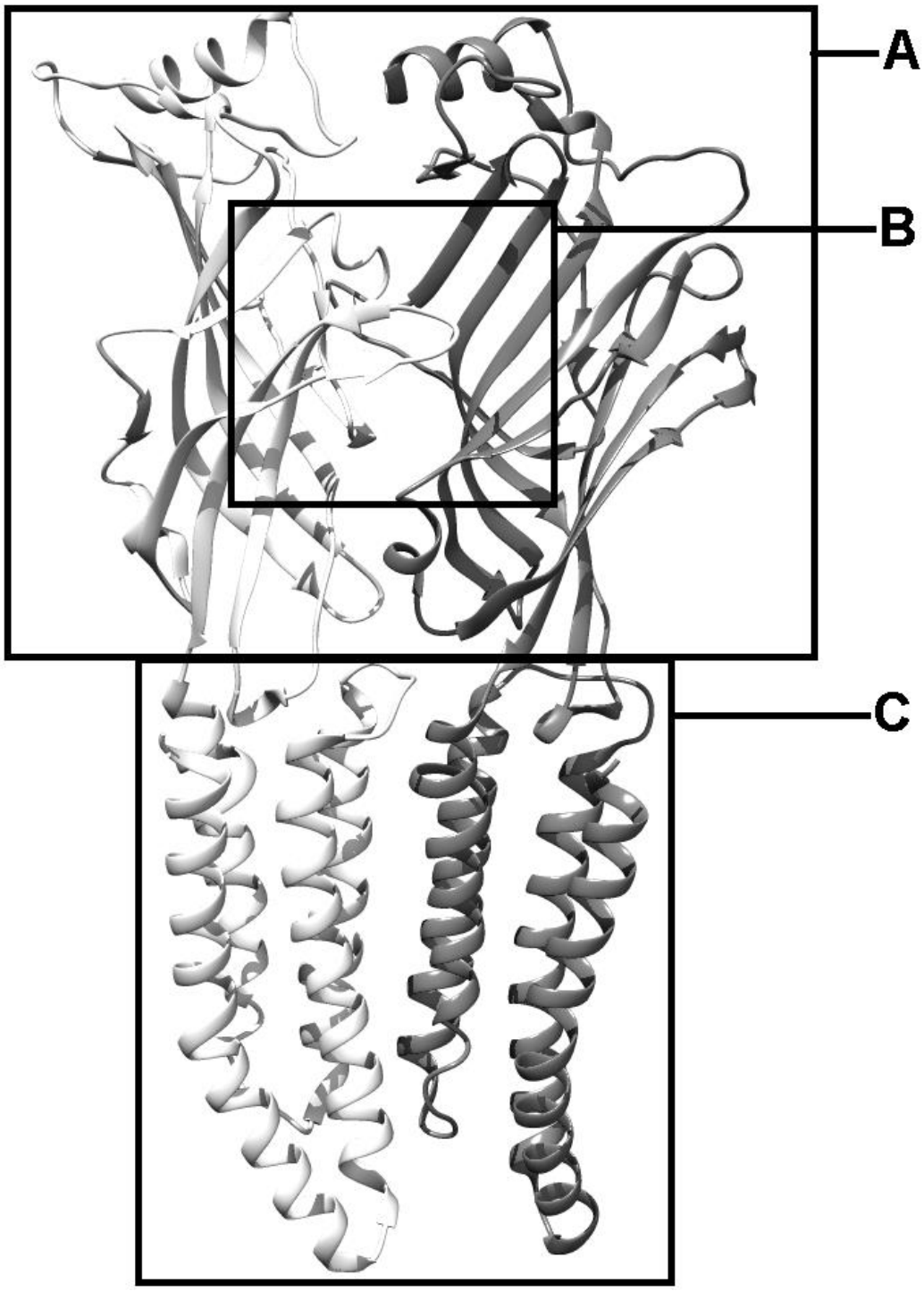

Figure 1.4 - A selection of two subunits of 3RIA interacting (representing a dimer) illustrating that within the extracellular domain **(A)**, a single functional agonist binding site **(B)** is found**.** The M1-4 domains **(C)** would be transecting the membrane of a cell, and a small portion of the protein would be accessible intracellularly (not shown).

1.3.2 Nematode LGICs

Caenorhabditis elegans has served as an excellent model organism for genetic comparison to other organisms (nematodes as well as mammals) for many reasons. Firstly, the full genome of *C. elegans* was sequenced in 1998, showing considerable conservation of genes with mammals. Secondly *C. elegans* has a very short life cycle, making it ideal for laboratory work. *C. elegans* contains the most extensive known superfamily of LGICs activated by many molecules such as acetylcholine, 5-HT_3, glutamate, GABA, glycine, as well as biogenic amines such as tyramine and dopamine. The super family of LGICs has been mainly divided into smaller families, including the groups: GGR-3, ACC-1, LGC-45, GGR-1, UNC-49, AVR-14, EXP-1, and the nicotinic acetylcholine receptors (nAChRs) (Jones and Sattelle, 2008). Indeed, studies on the functions of these receptors have highlighted their diversity. For example the AVR-14 group of receptors represent the glutamate-gated chloride channels which are the primary targets for the anthelmintic IVM (Cully *et al.* 1994). These receptors serve various functions in neurons in both *C. elegans* and *H. contortus* and play a key role in the regulation of pharyngeal pumping (Wolstenholme 2012). The GGR-3 group of ligand-gated chloride channels respond to biogenic amines such as serotonin (Ranganathan *et al.* 2000), dopamine (Ringstad *et al.* 2009; Rao *et al.* 2009) and tyramine (Pirri *et al*.2009) showing great ligand diversity in some of these families. The tyramine receptor LGC-55 appears to be involved in head movements in *C. elegans* (Pirri *et al.* 2009). The UNC-49 receptors are channels activated by GABA and are expressed in body muscles in *C. elegans* and are responsible for the sinusoidal movement of the worm which are key for coordinated movement (Bamber *et al.* 1999). These receptors appear to be pharmacologically distinct from mammalian GABA receptors as they don't respond to

classical GABA receptor antagonists (Accardi *et al.* 2012) and have a distinct agonist pharmacological profile (Kaji *et al.* 2015).

EXP-1 represent a unique type of GABA receptors which rather than conduct chloride ions instead conduct cations and are excitatory (Beg and Jorgensen, 2003). These receptors play a primary role in enteric muscle contraction responsible for defecation in *C. elegans* (Beg and Jorgensen, 2003). The ACC-1 group of receptors represent acetylcholine receptors that conduct chloride ions (Putrenko *et al.* 2005). The function of the GGR-1 and LGC-45 family is not yet known.

C. elegans and *H.* contortus are both nematodes from the same clade (clade V), and are therefore closely related genetically and share many of these diverse LGICs highlighted above. This makes it possible to find related LGIC subunits based on genetic homology between gene sequences of the two organisms. Additionally, the analysis of related LGICs in *H. contortus* will allow for some interesting comparisons between the function of LGIC orthologues between parasitic and free-living nematodes. An initial examination of the ligand-gated chloride channel family in *H. contortus* (Sanger Center Genome Project) in comparison to *C. elegans* indicated that most of the *LGCC* genes are conserved between the two organisms (Laing *et al.* 2013).

1.3.3 The acetylcholine-gated chloride channels (ACCs)

There are eight *acc* genes in this family for *C. elegans* with only seven appearing in the genome of *H. contortus*. These genes include ACC-1 to 4 and LGC-46 to 49 with LGC-48 not being found in the *H. contortus* genome. Very little is known about this family

of chloride channels, with only two studies published which identify and characterize these genes in *C. elegans* (Putrenko *et al.* 2005, Wever *et al.* 2015).

Putrenko *et al.* characterized the ACC-1 to ACC-4 genes in *C. elegans* noting that ACC-1 and ACC-2 were capable of forming homomeric channels in *Xenopus laevis* oocytes that respond robustly to acetylcholine and conducted chloride ions. Interestingly, the hallmark adjacent cysteines on loop C of the ligand binding α nAChR are absent in ACCs. The authors hypothesize that the ACCs have independently evolved an acetylcholine binding site, as residues in each binding loop between ACCs and nAChRs are not conserved. They show that both nicotine (the defining agonist of the nAChRs), as well as the related agonist cytisine, behave as weak agonists or antagonists of the ACCs.

Additionally, α-bungarotoxin had no effect on the ACCs, while being a potent competitive antagonist of the nAChRs by binding and interacting with loop C in those channels (Harel *et al.* 2001). It is also important to note that in *C. elegans,* ACC-4 was unable to form a functional homomeric channel. ACC-3 forms a heteromeric channel with ACC-1 *in vivo* which is less sensitive to acetylcholine and Wever *et al.* 2015 reported responses from ACC-3 homomeric channels to acetylcholine.

In addition, LGC-47 can form a functional channel *in vivo* with ACC-1. *In vivo* expression of the two subunits has been shown to overlap, particularly in the pharyngeal motor neuron M3 (Wever *et al.* 2015). The function of this neuron is to regulate pharyngeal pumping, particularly by promoting rapid relaxation of pharyngeal muscle tissue after a contraction, vital for effective transport of bacteria into the lumen of *C. elegans* (Avery and Thomas, 1997).

ACC-3 and ACC-4 seem to interact with ACC-2, as they were unable to obtain a response to acetylcholine in oocytes injected with either ACC-3/ACC-2 or ACC-4/ACC-2. Putrenko *et al.* (2005) hypothesize that perhaps ACC-3 and ACC-4 may negatively regulate ACC-2 *in vivo.* More likely, the authors suspect that the interaction of ACC-2 and either ACC-3 or 4 requires other additional subunits to form a functional channel *in vivo* (Putrenko *et al.* 2005).

More recently, there has been evidence that the ACC family of channels could be excellent anthelmintic targets (Wever *et al.* 2015). In this study open reading frame sequence of a GluCl subunit *avr-15* was cloned into vectors controlled by individual ACC subunit promoters. The AVR-15 subunit is sensitive to IVM, a macrocyclic lactone which acts by activating GluCls irreversibly. Using a strain of *C. elegans* that is resistant to IVM, and transforming these worms with this GluCl subunit directed to ACC expressing tissues, the effect of IVM could be tested on the physiology of the worms. They noted several very interesting results using this method. Firstly, they found that the construct directing AVR-15 to LGC-48 expressing tissue had little effect, so it could act as a control for further experimentation. Importantly, following exposure to IVM, the worms displayed a number of phenotypic effects. The effects included general lethality, inhibition of pharyngeal pumping rate, inhibition of egg laying, paralysis, and arrest of development. Moreover, worms expressing AVR-15 under of the control of the ACC-2, ACC-3, LGC-49, and LGC-47 promoters which are subsequently subjected to IVM treatments of 500 ng/mL, suffer severe deleterious effects, including death. Additionally, expression of AVR-15 in ACC-1 expressing tissue (e.g. the ventral nerve cord), resulted in paralysis from nM concentrations of IVM (Wever, *et al.* 2015).

These results along with the fact that the ACC family of channels are broadly expressed in *C. elegans* suggests that any drug that targets this family of channels would have good anthelmintic properties.

While it appears that the ACC family of subunits plays an important role in nematode biology, we still do not know their biological function in parasitic nematodes such as *H. contortus*. In addition, the binding site of ACCs appears to be very divergent compared to mammalian acetylcholine receptors. A detailed examination of the structure of the binding site and the mechanism of activation of the ACC family of *H. contortus* may unveil unique binding and activation mechanisms. This is important not only for rational drug design but also to help explain the evolution of the binding site of these receptors.

1.3.4 The binding site of LGICs

Most of the molecular details of the ligand-binding site of LGICs are based on studies of the acetylcholine binding proteins (AChBPs) from numerous organisms. The crystal structure of an AChBP was determined by x-ray diffraction by Brejc *et al.* 2001. They were able to resolve the structure to a 2.7Å resolution which generated a wealth of structural knowledge in terms of ligand binding and the shape of the ligand binding domain. The similarity between the AChBP and LGICs was confirmed by Dellasanti *et al.* in 2007, with an experiment where they crystallized the ligand binding domain of the α1 nicotinic acetylcholine receptor. The crystal structure of the AChBP also definitively showed that the ligand binding site is at the interface of 2 subunits which contribute a number of non-contiguous 'loops' that form an agonist binding pocket (Brejc *et al.* 2001). As more crystal structures of transmembrane channels become available, a clear picture of the structure-function relationship is beginning to resolve.

For example, an inhibitory anion selective LGIC from the nematode *C. elegans* has also been crystallized (Protein Data Bank accession 3RIA) (Hibbs *et al.* 2011). The *C. elegans* glutamate gated chloride channel (GluCl α) in complex with FAB, ivermectin, and L-glutamate was crystallized and the structure was mapped with a 3.3Å resolution via x-ray diffraction. This crystal structure has delivered a plethora of information about the interaction of drugs and endogenous ligands with inhibitory ion channels (Hibbs *et al.* 2011). The LGIC binding domain is comprised of the principal subunit, which contributes 3 of the peptide binding loops (A-C), and the secondary subunit, which contributes the remaining 3 (D-F) loops (β-sheets in this case) (Thompson *et al.* 2010) (Figure 1.5). The loops indicated in Figure 1.5 are based on homology modeling, and can vary between subunits, so, their locations in this case are only approximate.

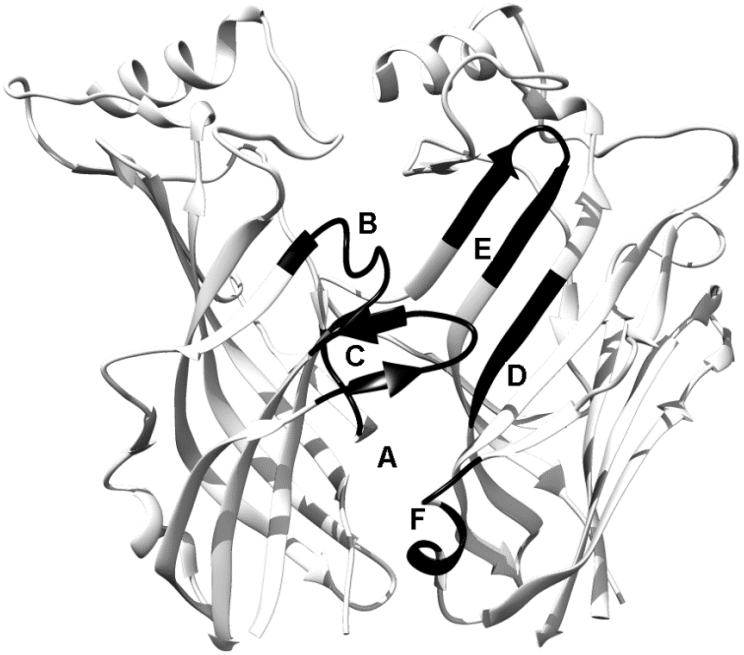

Figure 1.5 - Two ECD's (from the 3RIA crystal structure) illustrating the locations of the 6 major binding loops of one functional ligand binding site (A-F). Loops A, B, and C, are located on the primary subunit (left) and loops D, E, and F, are located on the secondary (right).

Generally, each loop will have 1-3 residues that line the binding pocket, with the remainder of the residues possibly playing other roles. The majority of the binding-pocket facing residues tend to have aromatic side chains and these aromatic amino acids contribute to what is known as the 'aromatic box'. This unit consists of approximately 4 aromatic resides that will surround an agonist at the time of binding (see Figure 1.6). This allows for the formation of strong π-cationic interaction which has been previously determined as essential for ligand-binding (Dougherty, 2008).

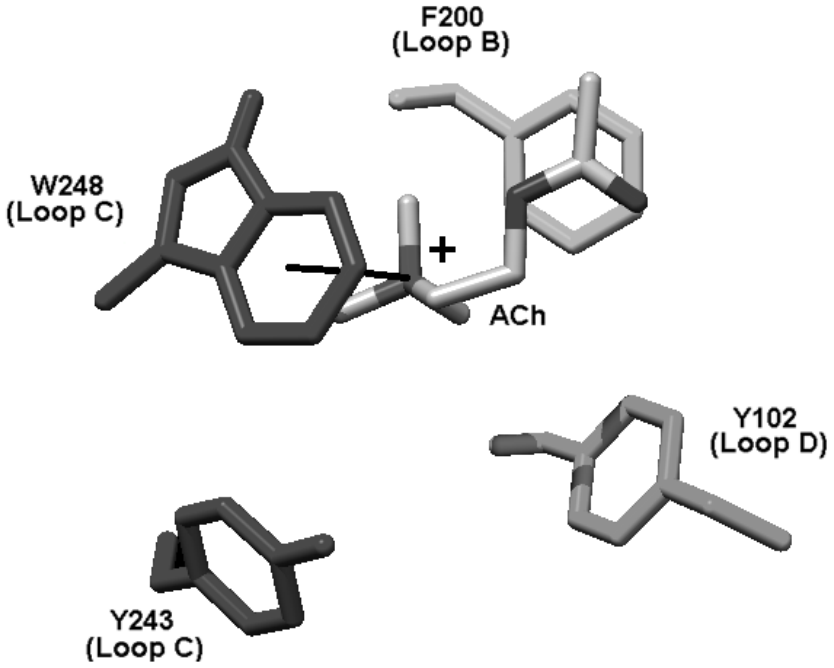

Figure 1.6 - A computer generated image of the Hco-ACC-2 aromatic box with ACh docked. This ligand docking simulation is explained further in section 3. This image shows the relative orientation of aromatic residues that are directly involved in agonist binding, with the hypothesized π-cationic interaction between the quaternary amine of ACh and the aromatic side chain of a tryptophan residue located in binding loop C.

The π-cationic interaction is generated by any of the 3 aromatic amino acids (Phe, Tyr, or Trp), and indeed, all 3 have been shown to be responsible for binding in different channels. For example, Beene *et al.* 2004, identified a π-cation interaction between serotonin and Trp183 in loop B in the 5-HT_3 receptor. However, it is Trp226 in loop C that forms a π-cationic interaction with serotonin in the MOD-1 serotonin receptor (Mu *et al.* 2003). Additionally, in the human glycine receptor, Phe159 in loop B is responsible for this interaction (Pless *et al.* 2008), while the interaction in the nAChR is with a Trp149 residue in loop B (Zhong *et al.* 1998). In the $GABA_C$ receptor, the π-cationic interaction occurs between GABA and Tyr198 in loop B (Lummis *et al.* 2005); while in the $GABA_A$ receptor, this bond occurs at Tyr97 in loop A (Padgett *et al.* 2007).

The strength of the potential π-cationic interaction depends on 2 factors, the nature of positive charge for the agonist, and, which aromatic residue is providing the π-cationic interaction. The strength of the π-cationic interaction depends on the electronegativity of the aromatic functional group, with Trp (indole functional group) having the greatest electronegativity, followed by Tyr and finally Phe. Molecules such as serotonin and acetylcholine tend to form these key π-cation interactions with Trp residues while GABA and glycine form these interactions with either Tyr or Phe residues.

It should be noted that different receptors that have the same endogenous agonist can have different binding mechanisms and orientations depending, in part, on the location of key aromatic residues (for example EXP-1 and UNC-49 both have the endogenous ligand GABA, but the binding sites are very different).

1.3.5 Rationale and objectives of the research

It is widely accepted that most of the currently used anti-parasitic drugs target ligand-gated ion channels. Thus, the identification of new LGICs that play an essential role in, for example, the neuromuscular system of the adult parasite may represent a good target for rational drug design. However, rational drug design requires a detailed knowledge of the binding site of these channels and their mechanisms of activation. As previously mentioned, the ACC-1 family of receptors appear to have potential as excellent nematocidal drug targets. However, genes encoding these channels have not been isolated or characterized in parasitic nematodes. Therefore the overall objective of this thesis is to isolate and partially characterize the ACC-1 family in the parasitic nematode *H. contorts*. This allowed us to begin the process of determining the importance of these channels in the parasite as future targets for novel antiparasitic drugs.

CHAPTER 2: METHODS

2.1 RNA isolation and cDNA production

Total RNA was isolated using Trizol (Invitrogen, Carlsbad, USA) from adult *Haemonchus contortus* strain PF23 supplied by Dr. Roger Prichard (Institute of Parasitology, McGill University). Copy DNA was synthesized using the Quantitect Reverse Transcription kit from Qiagen (Dusseldorf, Germany) using a unique 3' anchor sequence primer:

(5′CCTCTGAAGGTTCACGGATCCACATCTAGATTTTTTTTTTTTTTTTTVN3′);

[Where V is either A, C, or G and N is either A, C, G, or T] (Weston *et al.* 1999). The partial *H. contortus* sequence of *acc-1, acc-2 and acc-4* were initially identified by the Sanger Institute (Cambridge, UK) and used for the creation gene specific primers. These primers were used in the 5' and 3' Rapid Amplification of cDNA Ends (RACE) protocol (Frohman *et al.* 1988).

2.2 Semi-quantitative PCR Densitometry

Semi-quantitative PCR was conducted using primers specific for the *hco-acc-1* and *hco-acc-4* genes. Densitometry was conducted by measuring the fluorescence (AlphaImager, Alpha Innotech, USA) of ethidium bromide (Sigma) stained DNA bands under UV excitation. When the genes were amplified from cDNA produced from the reverse transcription of relevant life stage RNA (1 µg RNA to final volume of 25 µL), the fluorescent signal was normalized against the fluorescence of the β-tubulin housekeeping gene which was amplified and arrested at the same PCR cycle.

2.3 Isolation of *hco-acc-1, hco-acc-2, hco-acc-4*

The cloning of all genes was performed by the (RACE) procedure (Frohman *et al.* 1994) and the same approach. As an example, the 5' end of the *hco-acc-1* gene was amplified using two internal *hco-acc-1* specific antisense primers [NESTED PRIMER 5' GTTGTTCCAAACGCACCTGTGG 3'] and a primer specific for splice leader – 1 sequence (SL1-5′GGTTTAATTACCCAAGTTTGAG3′) (Van Doren and Hirsch, 1988) in a PCR using the PTC-100 Programmable Thermal Controller (MJ Research, Inc, Waltham, MA, USA). For the 3' end, two *hco-acc-1* (or *hco-acc-2/hco-acc-4)* gene specific primers and primers specific for the 3' oligo-dT anchor sequence were used in a nested PCR reaction. Each amplicon of a predicted size was isolated via gel extraction and subcloned into the pGEMT easy™ vector and subsequently sequenced.

Amplification of the complete *hco-acc-1* (or *hco-acc-2/hco-acc-4)* gene was conducted using primers designed targeting 5' and 3' untranslated region. These amplicons were subcloned and sequenced to achieve a consensus sequence for each gene separately. Sequence alignments and analysis were performed using Clustal Omega (Larkin *et al.,* 2007).

2.4 Expression of ACC-2 *Xenopus laevis* oocytes

All animal procedures followed the University of Ontario Institute of Technology Animal Care Committee and the Canadian Council on Animal Care guidelines. *Xenopus laevis* frogs (all female) were supplied by Nasco (Fort Atkinson, WI, USA). The frogs were housed in a room which was climate controlled, light cycled, and stored in tanks which were regularly cleaned.

Frogs were anesthetized with 0.15% 3-aminobenzoic acid ethyl ester methanesulphonate salt (MS-222) buffered with $NaHCO_3$ to pH 7 (Sigma-Aldrich, Oakville, ON, CA). Surgical removal of a section of the ovary of the frog was performed, and the lobe was defolliculated with a calcium-free oocyte Ringer's solution [82 mM NaCl, 2 mM KCl, 1 mM $MgCl_2$, 5 mM HEPES pH 7.5 (Sigma-Aldrich)] (OR-2) containing 2 mg/mL collagenase-II (Sigma-Aldrich). The oocytes in the defolliculation solution were incubated at room temperature for 2h. Collagenase was washed from the oocytes with ND96 solution (1.8 mM $CaCl_2$, 96 mM NaCl, 2 mM KCl, 1 mM $MgCl_2$, 5 mM HEPES pH 7.5) and oocytes were allowed one hour to recover at 18°C in ND96 supplemented with 275 µg ml^{-1} pyruvic acid (Sigma-Aldrich) and 100 µg ml^{-1} of the antibiotic gentamycin (Sigma-Aldrich). Stage V and VI oocytes were selected for cytoplasmic injection of cRNA.

The coding sequence of *hco-acc-2 was* subcloned into the *Xenopus laevis* expression vector pGEMHE (Zhang *et al.* 2008). The vector was linearized using the restriction enzymes *NheI* (New England Biolabs, USA), and used as template for an *in vitro* transcription reaction (T7 mMessage mMachine kit, Ambion, Austin, TX, USA) yielding *hco-acc-2* copy RNA. *Xenopus laevis* oocytes were injected with 50 nL of *hco-acc-2* (0.5 ng/nL) using the Drummond (Broomall, PA, USA) Nanoject microinjector.

The injected oocytes were incubated at 18°C in ND96 (96 mM NaCl, 2 mM KCl, 1 mM $MgCl_2$, 1.8 mM $CaCl_2$, 5 mM HEPES pH 7.5) supplemented with 0.275 µg/mL pyruvate and 50 µg/mL gentamycin. Electrophysiological recordings of the oocytes were conducted between 48 and 72 hours after cRNA injection.

2.5 Electrophysiological recordings

The Axoclamp 900A voltage clamp (Molecular Devices, Sunnyvale, CA, USA) was used to conduct two electrode voltage clamp electrophysiology. Glass electrodes were produced using a P-97 Micropipette Puller (Sutter Instrument Co. Novato, CA, USA). The electrodes were backfilled with 3M KCl and contained Ag|AgCl wires, and electrodes with resistances of 1-8 MΩ were selected for recordings. All oocytes were clamped at -60 mV for the entirety of the experiments. Acetylcholine (Sigma- Aldrich) was first dissolved in ND96.

The resultant solutions were perfused over oocytes using the RC-1Z recording chamber (Warner Instruments Inc., Hamdan, CT, USA). Data was subsequently analyzed using Clampex Software v10.2 (Molecular Devices) and all graphs were generated using Graphpad Prism Software v6.0 (San Diego, CA, USA). Acetylcholine EC_{50} value was determined by dose response curve fit to the equation:

$$I_{max} = \frac{1}{1 + \left(\frac{EC_{50}}{[D]}\right)^{h}}$$

Where I_{max} is the maximal response, EC_{50} is the concentration of compound required to elicit 50% of the maximal response, [D] is compound concentration, and *h* is the Hill coefficient. Both EC_{50} and *h* are free parameters, and the curves were normalized to the estimated I_{max}. Graphpad Prism used the equation to fit a sigmoidal curve of variable slopes to the data.

2.6 *In silico* homology protein modelling

To allow for comparison between the acetylcholine binding sites of Hco-ACC-1, Hco-ACC-2, and Hco-ACC-4, the crystal structure of the protein 3RIA was selected as the template to model the homodimers. 3RIA is an inhibitory anion-selective cys-loop homopentameric *C. elegans* glutamate-gated chloride channel, whose structure was determined at a 3.3 Å resolution (Hibbs *et al.* 2011). The X-ray structure of the GluCl-Fab complex was determined with the allosteric agonist ivermectin and with the endogenous neurotransmitter L-glutamate. This selection was chosen based on total subunit sequence homology and alignment as determined by PHYRE 2 (Kelley *et al.* 2015).

The entire query subunit amino acid sequences of all the ACC subunits were searched to verify that 3RIA would serve as the optimal template for each ACC. The 3RIA amino acid sequence was then used alongside the ACC sequences in automated scripts run by MODELLER v9.15 (Sali and Blundell, 1993) for the generation of the Hco-ACC-1, Hco-ACC-2, and Hco-ACC-4 extracellular domain homodimers.

The most energetically favourable models based on DOPE scores were selected and subjected to PROCHECK Ramachandran plot analysis. Model analysis and molecule distance measurements were conducted using USCF Chimera v1.10.2 (Pettersen *et al.,* 2004).

2.7 Computational agonist docking

Ligands were obtained from the Zinc database http://zinc.docking.org/ (Irwin *et al*., 2012) in their energy reduced form. Hco-ACC-1, Hco-ACC-2, and Hco-ACC-4 homodimer models were prepared for ligand docking using AutoDock tools (Morris *et al.* 2009). This preparation includes the addition of polar hydrogens which are not present in the dimer generated by MODELLER nor in the energy reduced form from the Zinc database. This procedure allows for the consideration of potential hydrogen bonds when the program attempts to dock the ligand to receptor. AutoDock Vina (Trott and Olson, 2010) was used for simulated docking of prepared ligands to the dimers. A 30x30x30 Å search cube was centered at the location of the aromatic box of the homodimer models. From this, 50 binding models within a range of 5 kcal·mol^{-1} of the best scoring dock were generated.

2.8 Immunolocalization of ACC-1 in *H. contortus*

A peptide specific for a portion of the N-terminal region of the Hco-ACC-1 protein (YNKHYIPSHPTQVRVDM) was synthesized commercially, (21st Century Biochemicals, Marlboro, MA, USA) and was used to immunize rabbits. The peptide was conjugated to the carrier protein ovalbumin and was BLASTed against the *H. contortus* genome database and the NCBI general database to ensure specificity. Antibodies were tested for specificity and titer against the immunogenic peptide by ELISA, this process included analysis of cross reactivity between the specific antibodies and all the peptides used in antibody production. Two strains of *H. contortus* were used: PF23 and MOF23. Both strains were derived from the same parental strain. The PF23 strain was generated by passage through sheep over 23 generations without anthelmintic treatment whereas MOF23 was generated by passage through sheep over 23 generations with increasing dosage of moxidectin at each generation. Further details of the strains can be found in

Urdaneta-Marquez *et al.* 2014. Adult female *H. contortus* worms (strains PF23 and MOF23) were fixed, permeabilized and subsequently digested as previously described (Rao *et al*. 2009).

Worms were subsequently washed 3 times with PBS, and incubated at 4°C for 72 hours with a 1/150 dilution of primary antibody diluted in 0.1% w/v BSA, 0.5% Triton X-100, and 0.05% sodium azide (Sigma) under slight shaking. The removal of unbound antibodies was conducted by 4 washes of the worms with PBS and a final wash with PBS with 0.1% (v/v) Triton X-100 (PBST). Worms were then incubated at 4°C with a 1/2000 Alexa Fluor® goat anti-rabbit IgG (H+L) secondary, for 24h. Unbound secondary antibody was removed by 4 washes of the worms with PBS, and a final PBST wash. Worms were mounted on slides using Fluoromount™ Aqueous Mounting Medium (Sigma) and examined. Slides were examined using a Zeiss LSM710 confocal microscope (Carl Zeiss Inc., Canada) equipped with the Zeiss Zen 2010 software package. The lasers used for image acquisition were an Argon 488 nm, with the filter sets adjusted to minimize bleed-through due to spectral overlap.

Several controls were conducted including the omission of primary antibody, a pre-immune control (where 1/50 dilutions of pre-immune serum from experimental rabbits was applied instead of the purified primary antibody), and, a peptide absorbed control (where an excess of peptide (50ug/ml) was added to the primary antibody dilution and incubated for 24h at 4°C before immunocytochemistry).

CHAPTER 3: RESULTS

The original rationale for choosing the ACC-1 family for further examination in *H. contortus* was previous knowledge of their importance as drug targets from research on the model nematode *C. elegans* (Wever et al 2015). In addition to this information, an initial examination of gene transcripts in *H. contortus* indicated that these genes, particularly *acc-1* appeared to be prominent in the adult stage compared to other genes for ligand-gated chloride channels (Figure 3.1A). This readily amplified gene and associated family were then chosen for further characterization. Densitometric readings were taken from end-point PCR (arrested during linear amplification of the genes) as a semi-quantitative measure of relative expression during each life-stage.

Figure 3.1 C shows a very similar level of expression of *hco-acc-1* during both the adult and larval life-stages. There is a notable difference of expression for *hco-acc-4,* wherein the L3 larval stage shows a greater expression of the gene compared to the adult life-stage.

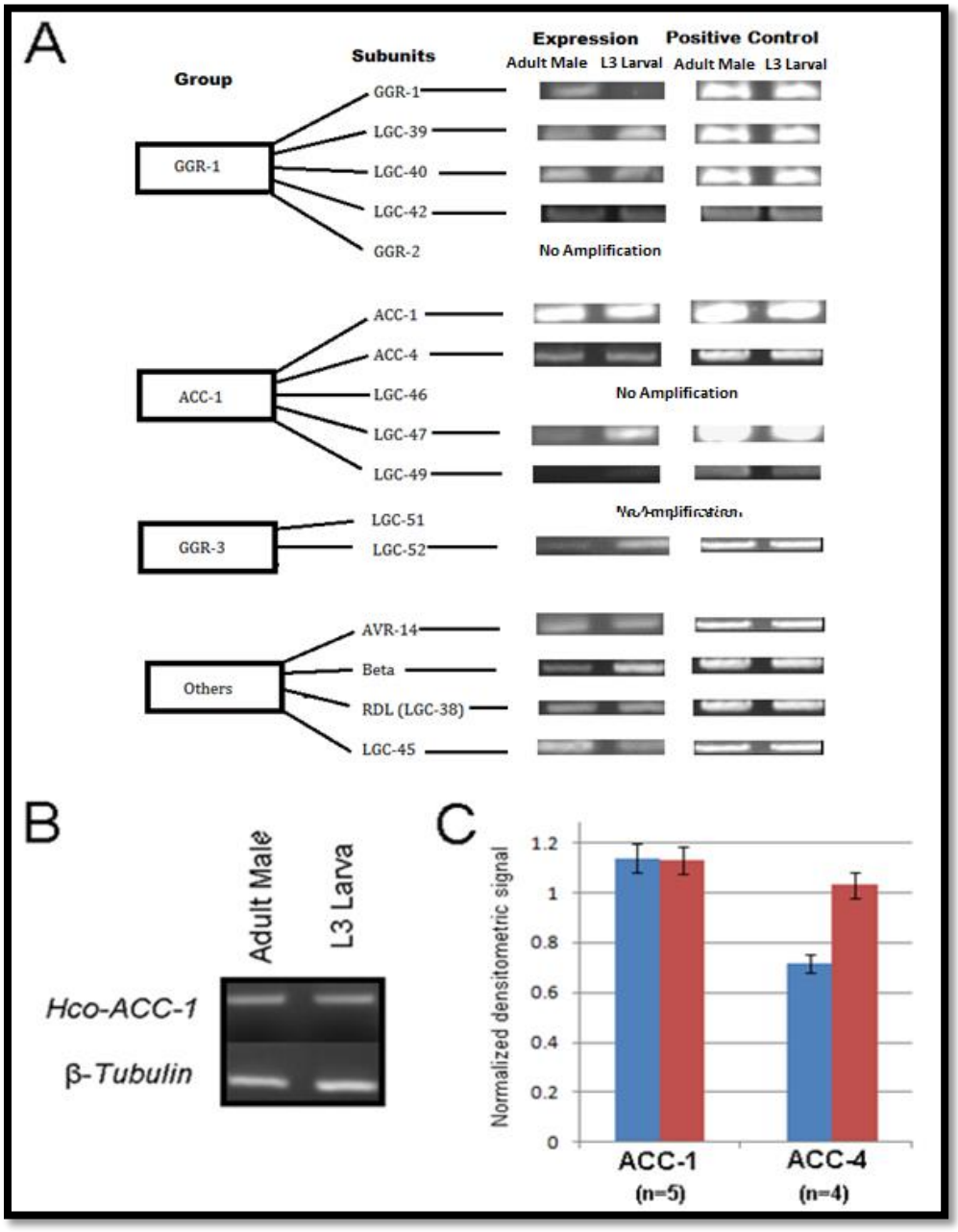

Figure 3.1 – (A) Initial end-point PCR amplification of a number of different genes from L3 larval and adult male *H. contortus* cDNA compared to the amplification of the β-tubulin housekeeping gene. **(B)** Example of PCR amplification arrested before linear amplification has ended for *hco-acc-1*. **(C)** Densitometric readings based on linear amplification arrest (semi-quantitative PCR) for hco-acc-1 and hco-acc-4. For both genes, the left bar is amplification from adult male cDNA and the right bar is amplification from L3 larval cDNA.

3.1 Isolation and characterization of *hco-acc-1, hco-acc-2, and hco-acc-4*

The final consensus nucleotide product for *hco-acc-1* obtained through the RACE procedure was sequenced and shown to consist of 1380 nucleotides and was submitted to GenBank (accession number KC918363.1). When translated in the appropriate reading frame, the sequence encodes a protein containing 459 amino acids with the hallmark cys-loop motif (Figure 3.2). A homodimer of Hco-ACC-1 was generated using *in silico* protein homology modelling using the nematode GluCl crystal structure (3RIA) as a template (Figure 3.3). The model of the 2 subunits was used to perform *in silico* ligand docking simulations and depicts the dimer interacting with acetylcholine.

Additionally, 4 hydrophobic transmembrane domains were identified along with a signal peptide cleavage site between residues 22 and 23 (Signal P). The PAR motif (residues 268-270) (Figure 3.2) was noted in the M2 transmembrane portion of the peptide, indicative of chloride ion selectivity (Jensen *et al.* 2005). The Hco-ACC-1 peptide shares an 89% homology with the *C. elegans* ACC-1 subunit (Figure 3.3). A few key amino acid differences were noted in the major binding loops. Firstly, in ligand binding loop C, a tyrosine (Y178) was identified in the Hco-ACC-1 protein where a phenylalanine (F179) was seen in the analogous position in Cel-ACC-1. Secondly, there are two differences seen in binding loop F. In Hco-ACC-1 two positions, P199 and Q201, align to R200 and E201, in Cel-ACC-1 (Figure 3.3).

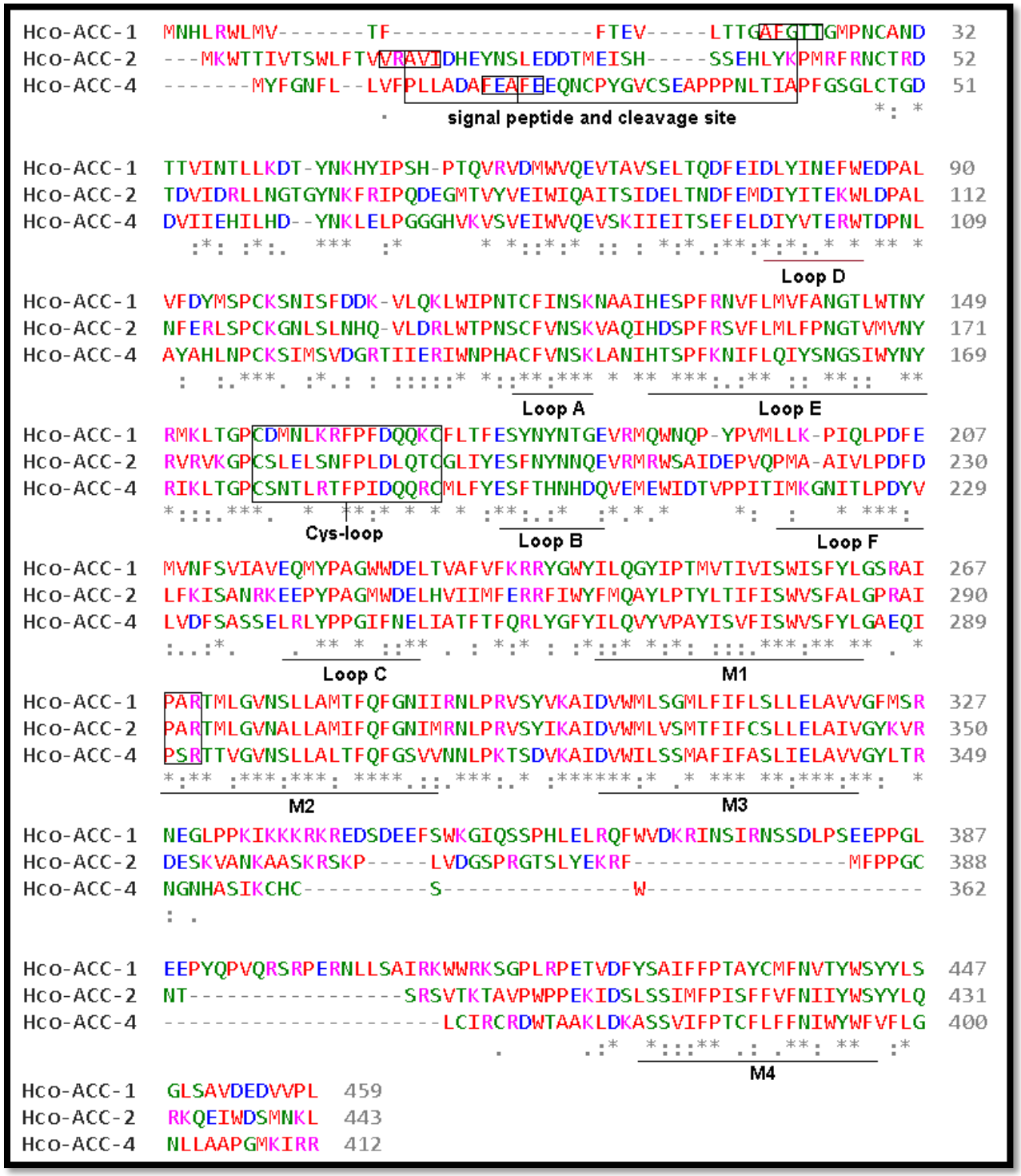

Figure 3.2 - Clustal Omega multiple sequence alignment of the amino acid sequences of Hco-ACC-1, Hco-ACC-2, and Hco-ACC-4. Alignment highlights signal peptides (and cleavage sites) the cys-loop, binding loops (A-E) as well as the M1-M4 transmembrane domains.

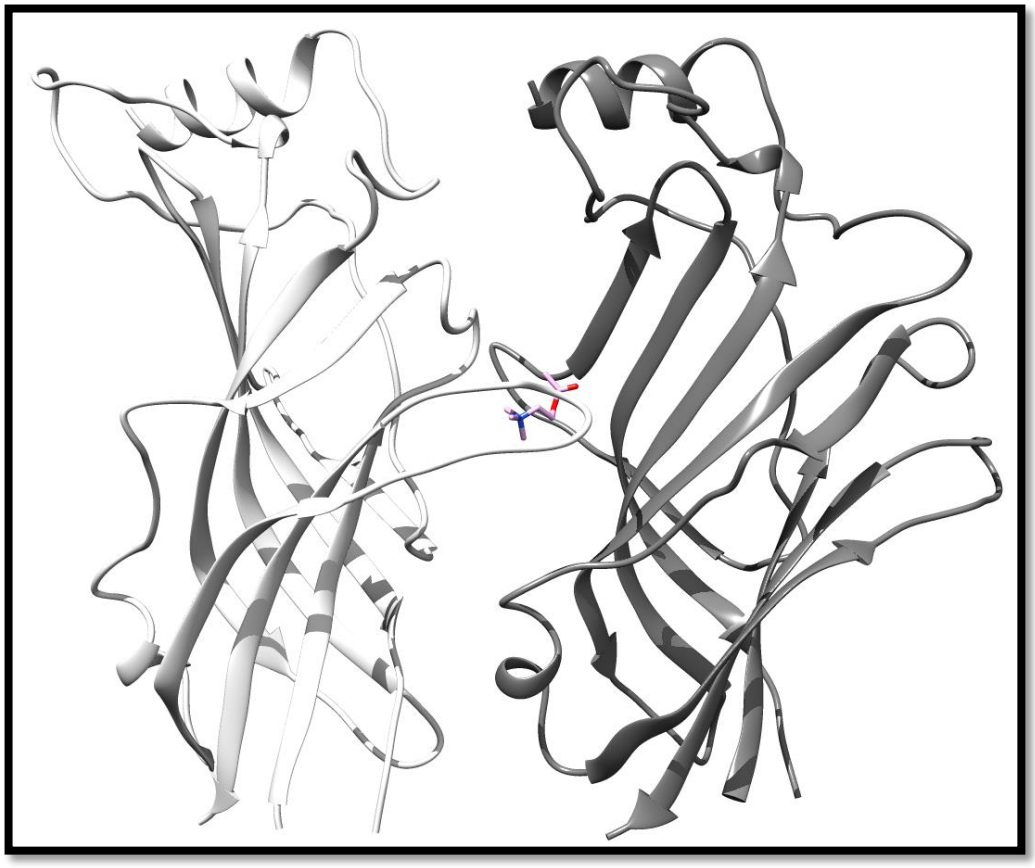

Figure 3.34 - Homology model of Hco-ACC-1 based on the nematode GluCl crystal (3RIA). A homodimer (primary subunit on the left, complementary subunit on the right) is displayed with acetylcholine docked accomplished with AutoDock Vina.

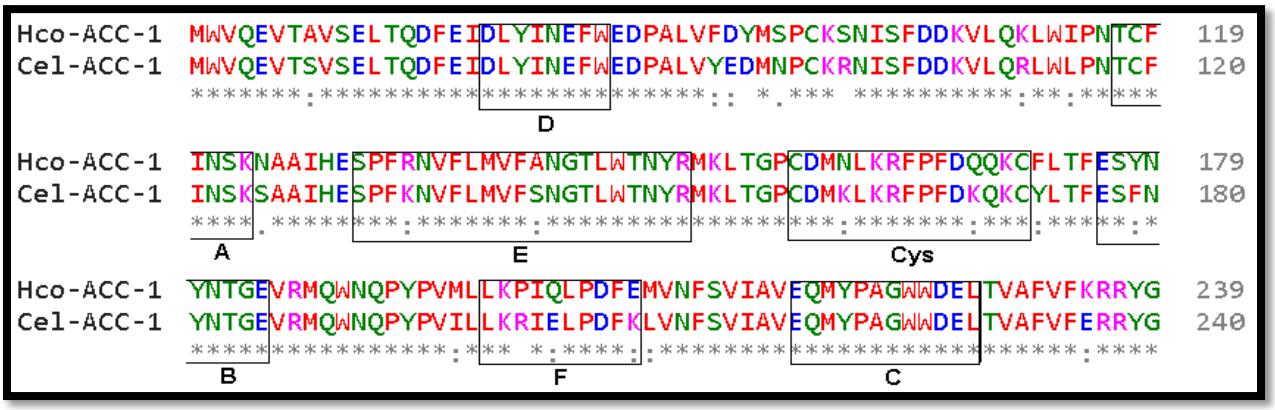

Figure 3.4 - Clustal Omega alignment between Hco-ACC-1 and Cel-ACC-1 specifically focusing on the extracellular domain. The cys-loop as well as the major binding loops (A-E) have been highlighted for comparison.

The final consensus nucleotide product for *hco-acc-2* obtained through the RACE procedure was sequenced and shown to consist of 1332 nucleotides and was submitted to GenBank (accession number KC918364.1).When translated in the appropriate reading frame, the sequence encodes for a protein containing 444 amino acids with the hallmark cys-loop motif (Figure 3.2). A homodimer of Hco-ACC-2 was generated using *in silico* protein homology modelling using the nematode GluCl crystal structure (3RIA) as a template (Figure 3.5).

This dimer was used to perform *in silico* ligand docking simulations and depicts the 2 subunits interacting with acetylcholine. In addition, 4 hydrophobic transmembrane domains were identified along with a signal peptide cleavage site between residues 17 and 18 (Signal P). The PAR motif (residues 266-268) (Figure 3.2) was noted in the M2 transmembrane portion of the peptide, indicative of chloride ion selectivity (Jensen *et al*. 2005). The Hco-ACC-2 peptide shares an 83% homology with the *C. elegans* ACC-2 sequence (Figure 3.6).

A few key amino acid differences were noted in the major binding loops. Firstly, in ligand binding loop D, a Lysine (K106) was identified in the Hco-ACC-2 protein sequence where a threonine (T104) is seen in the analogous position in Cel-ACC-2. Secondly, there is a major difference in binding loop F, wherein the Hco-ACC-2 protein, an alanine exists (A222) that aligns to an arginine in the analogous position (Figure 3.5).

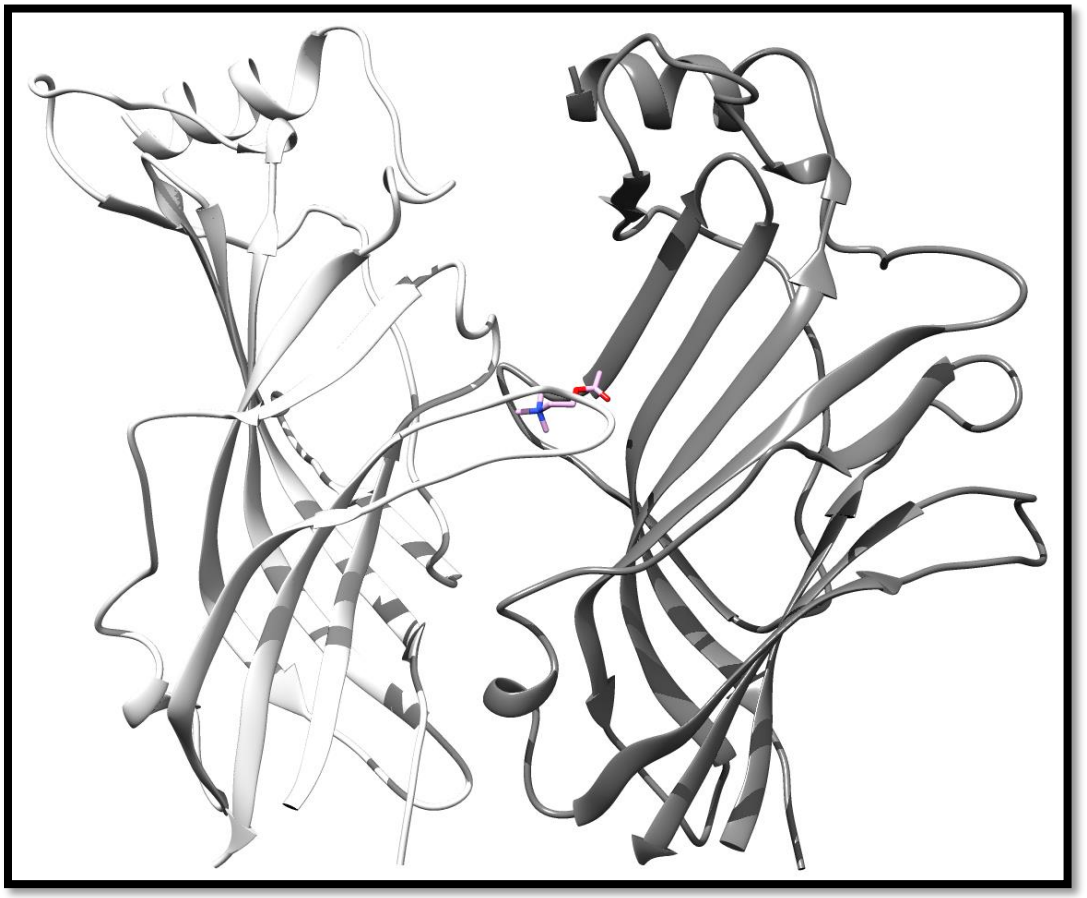

Figure 3.6 - Homology model of Hco-ACC-2 based of the nematode GluCl crystal (3RIA). A homodimer is displayed with acetylcholine docked accomplished with AutoDock Vina.

Figure 3.5 - Clustal Omega alignment between Hco-ACC-2 and Cel-ACC-2 specifically focusing on the extracellular domain. The cys-loop as well as the major binding loops (A-E) have been highlighted for comparison.

The final consensus nucleotide product for *hco-acc-4* obtained through the RACE procedure was sequenced and shown to consist of 1200 nucleotides and was submitted to GenBank (accession number KC918365.1). When translated in the appropriate reading frame, the sequence encodes for a protein containing 400 amino acids highlighted by the signature cys-loop motif (Figure 3.2). A homodimer of Hco-ACC-4 was generated using *in silico* protein homology modelling using the nematode GluCl crystal structure (3RIA) as a template (Figure 3.7). The simulated dimer was used to perform *in silico* ligand docking simulations and depicts the dimer interacting with acetylcholine.

Additionally, 4 hydrophobic transmembrane domains were identified along with a signal peptide cleavage site between residues 19 and 20 (Signal P). The PAR motif is modified in Hco-ACC-4, and is instead PSR (residues 289-291) in the M2 transmembrane portion of the peptide (Figure 3.2). The Hco-ACC-4 peptide shares a 91% homology with the *C. elegans* ACC-4 subunit (Figure 3.8). The only potentially significant differences noted between the *H. contortus* and *C. elegans* ACC-4 peptides appears to be in binding loop E, where a tyrosine in Hco-ACC-4 is aligned to a histidine in the Cel-ACC-4 peptide. Additionally, on the other end of binding loop E, a threonine is aligned to a glutamine (Hco-ACC-4 and Cel-ACC-4 respectively) (Figure 3.7).

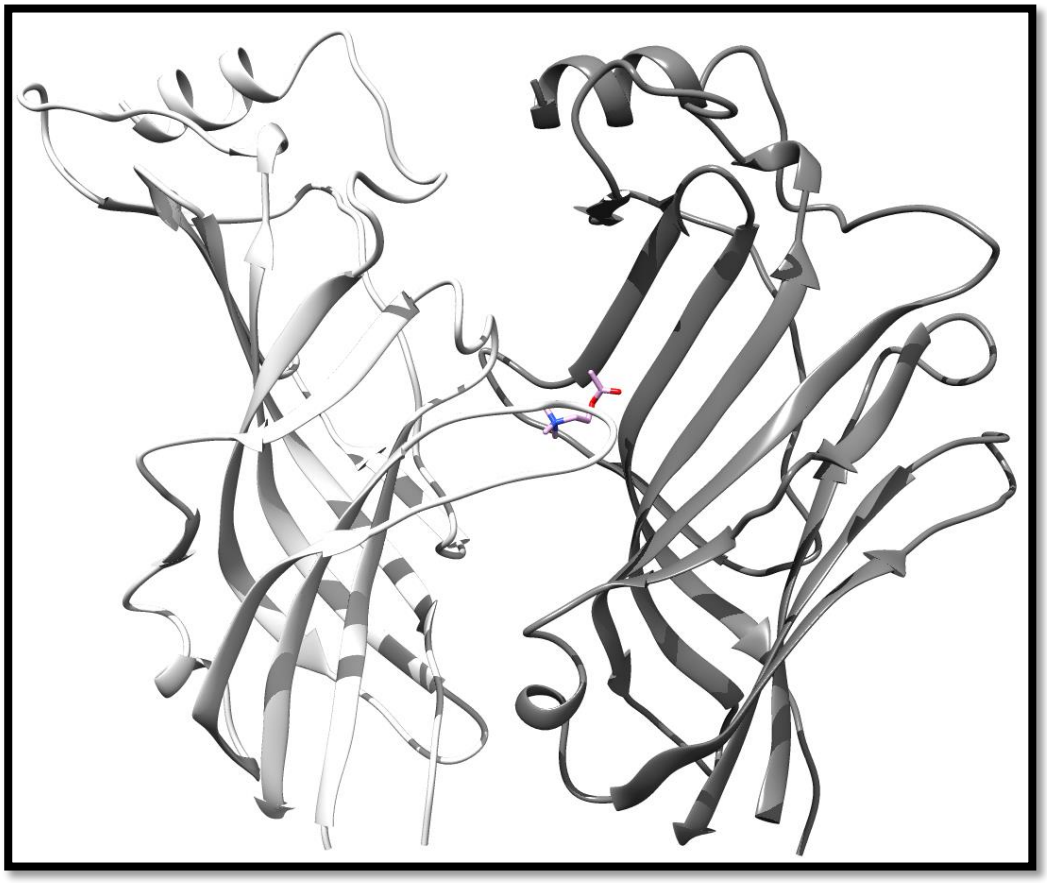

Figure 3.8 - Homology model of Hco-ACC-4 based of the nematode GluCl crystal (3RIA). A homodimer is displayed with acetylcholine docked accomplished with AutoDock Vina.

Figure 3.7 - Clustal Omega alignment between Hco-ACC-4 and Cel-ACC-4 specifically focusing on the extracellular domain. The cys-loop as well as the major binding loops (A-E) have been highlighted for comparison.

Interestingly, while Hco-ACC-1 and Hco-ACC-2 both contain a tryptophan residue located in loop C, which is also conserved amongst the Cel-ACC-1 and Cel-ACC-2 sequences, neither species version of ACC-4 contains a tryptophan residue within binding loop C (Figure 3.2). Also, interesting is the inherent short length of the ACC-4 genes in both *H. contortus* as well as *C. elegans* genome. Based on alignments between Hco-ACC-1, Hco-ACC-2, and Hco-ACC-4, it appears that a major section of the genes that code for the protein are missing. Based on the alignment of the 3 translated genes (Figure 3.2) a significant portion of the intracellular loop of the peptide located between the M3 and M4 transmembrane domains is not present (Figure 3.2).

3.2 Electrophysiological analysis of Hco-ACC-2

Hco-ACC-2 forms a homomeric acetylcholine gated channel in oocytes that responds robustly to acetylcholine as well as nicotinic agonists, carbachol, urecholine, arecholine, choline and nicotine (Figure. 3.9A). Carbachol applied at a dosage of 500 µM achieved a % maximal ACh response of 102.3% ± 4.6%. Urecholine applied at the same dosage managed a % max response of 81.5% ± 3.8%. Arecoline, choline and nicotine generated smaller % max responses (compared to ACh) at 51.2% ± 1.3%, 26.3% ± 1.8%, and 12.1% ± 0.3%, respectively (Figure 9B). Dose-response experiments using increasing concentrations of acetylcholine revealed an EC_{50} of 21.98 ± 1.53 µM and a Hill Coefficient of 1.63 ± 0.24 (Figure 3.10).

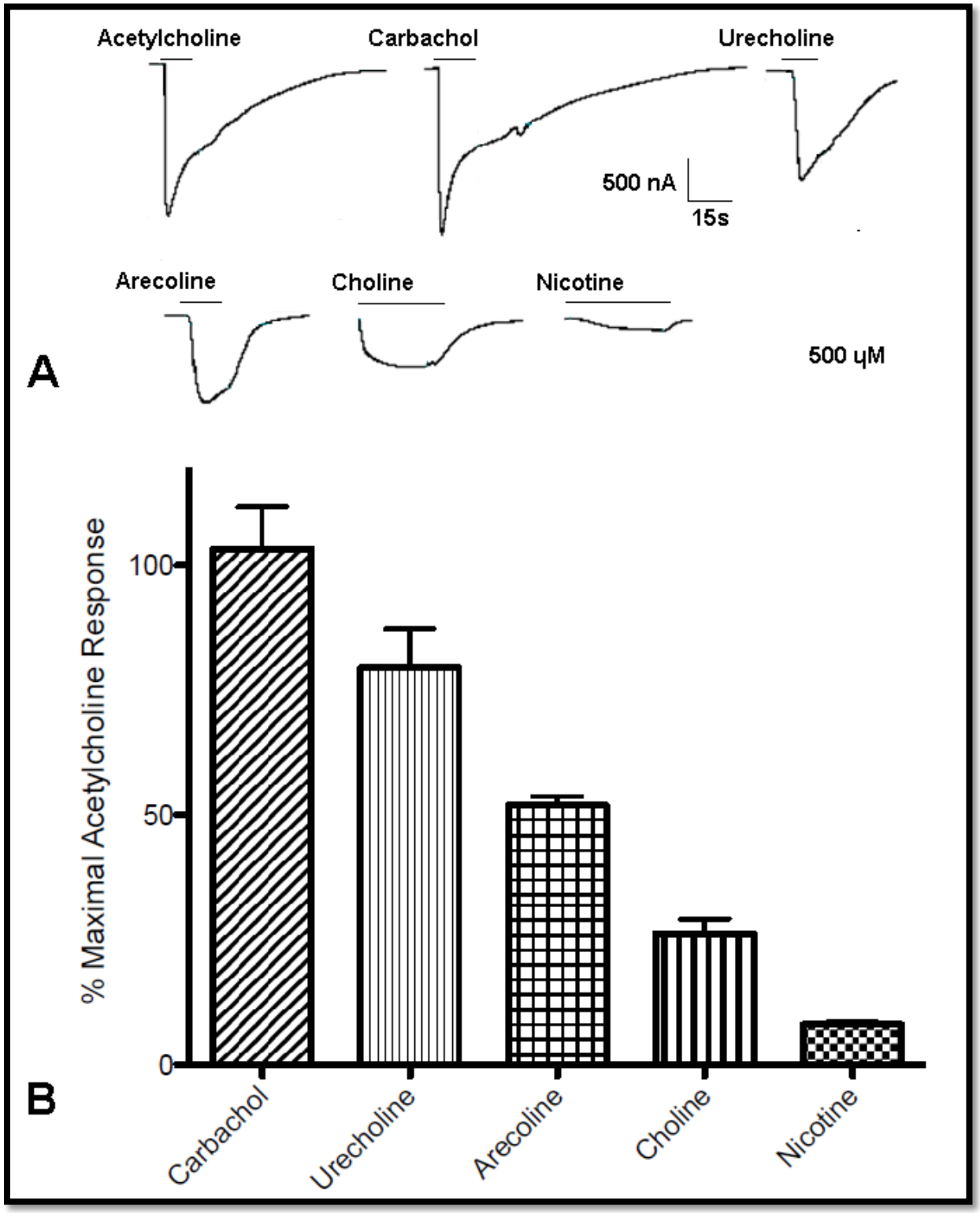

Figure 3.9 – (A) Representative tracings of Hco-ACC-2 receptors functionally expressed in *X. laevis* oocytes exposed to a variety of agonists. All agonists were tested a [500 µM], which exceeds the concentration of acetylcholine required to achieve a maximal response. Similar results were seen for each compound on multiple oocytes. (B) The

percent response achieved by the application of 500 µM of selected agonists on *X. laevis* oocytes expressing Hco-ACC-2 (n=6) compared to the maximal response achieved by 500 µM ACh.

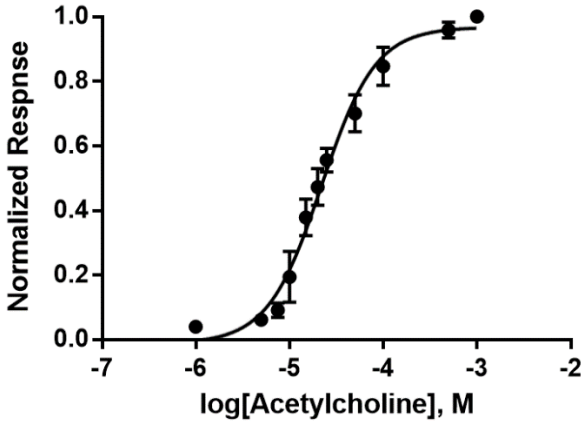

Figure 3.10 - Hill curves fit to data collected by exposing oocytes injected with *hco-acc-2* RNA (n=6) to increasing concentrations of ACh. Error bars represent ± standard error.

3.3 Immunolocalization of Hco-ACC-1

The application of anti-Hco-ACC-1 antibodies was performed on adult female *H. contortus* worms to determine the tissue expression of the ACC-1 protein. Worms from both the PF23 and MOF23 strains were selected and successfully stained, with repeated staining over multiple batches of collected worms. The signal was identified consistently in pharyngeal muscle cells, in the anterior half of the pharynx, in both strains and also in pharyngeal tissue isolated from worms (Figure 3.11 A-D). There were no obvious differences in the signal between *H. contortus* strains. The observed signal was robust and reconstructed stacks of slices through the Z axis shows the tri-radiate organization of nematode pharyngeal muscle (Figure 3.11). Peptide absorbed controls, pre-immune serum controls and controls without primary antibody displayed no signal beyond background (Figure 3.11 E and F).

The *H.* contortus adult pharynx appears as a single tube with a small pseudo-bulb present in the posterior half (Figure 3.11). The posterior half of the pharynx meets the gut directly, but no obvious terminal bulb is present. Rather, the diameter of the pharynx appears to gradually enlarge moving posteriorly from the pseudo-bulb (Figure 3.11).

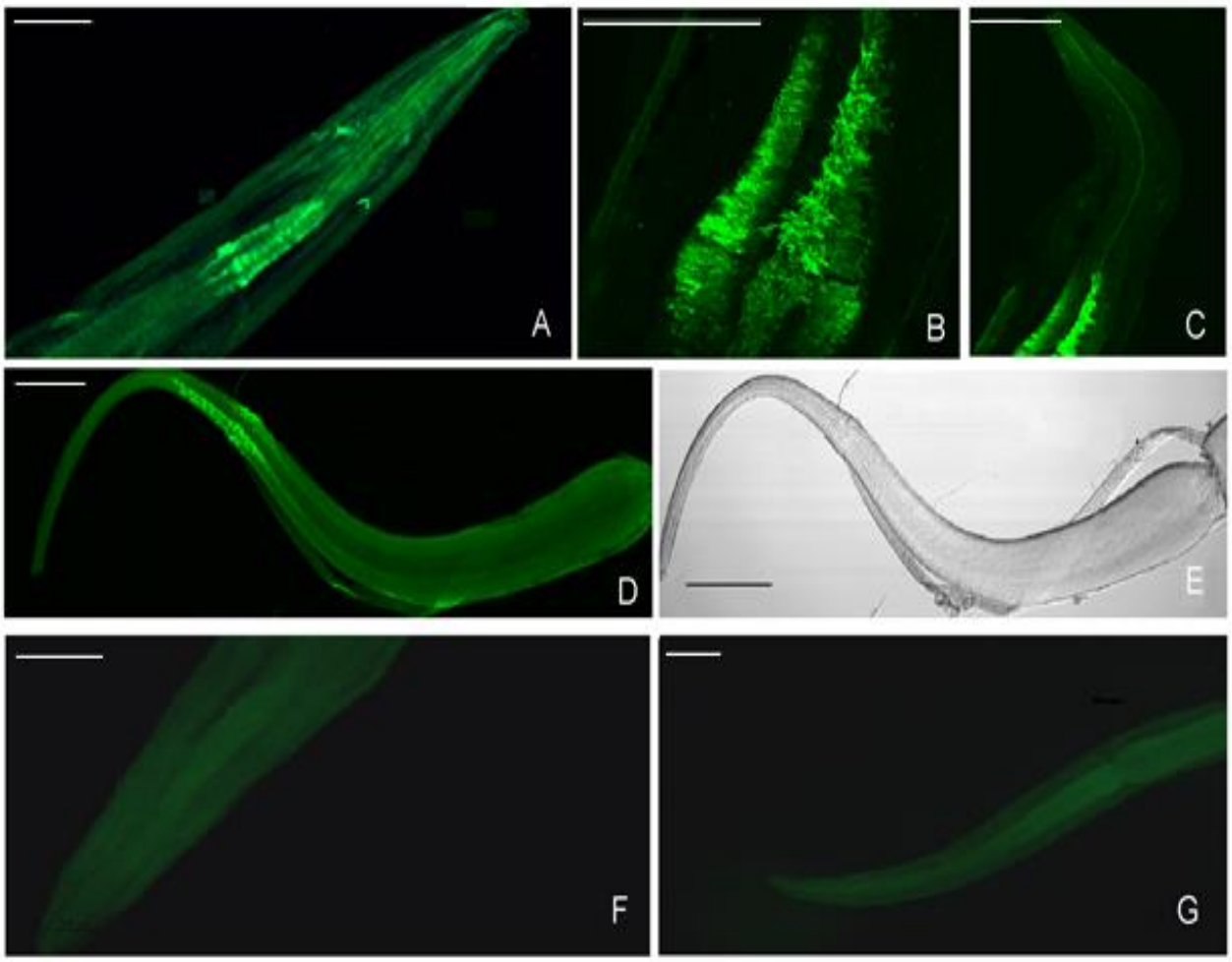

Figure 3.11 - Immunolocalization of Hco-ACC-1 in adult female *H. contortus* worms. **(A)** 25x magnification of the anterior end of *H. contortus* PF23 strain. **(B)** 40X magnification stack of 25 of 5µm confocal slices of *H. contortus* PF23 focused on the anterior half of the pharyngeal muscle tissue. **(C)** 25x magnification of a female adult *H. contortus* MOF23 parasite focusing on the anterior end of the worm. **(D)** 25x magnification of isolated pharynx from a female *H. contortus* MOF23 adult worm. **(E)** 25x magnification light micrograph of D. **(F)** Pre-immune serum negative control of *H. contortus* PF23, 25x magnification focusing on anterior end of the worm. **(G)** Peptide-absorbed control of *H. contortus* MOF23 at 10x magnification focusing on the anterior end of the worm. Lines denote 100 µm.

3.4 *In silico* homology protein modelling

Optimal protein modelling results were obtained from models generated using the 3RIA crystal as a template. Key binding differences between Hco-ACC-1, Hco-ACC-2, and Hco-ACC-4 are summarized in Figure 3.12. Interestingly, acetylcholine has been simulated to form π-cationic bonds with the Trp residue found in loop C of ACC-1 and ACC-2, but also with the analogous Phe found in ACC-4. Proximity of the positively charged quaternary amine group of acetylcholine to the center of the aromatic rings of loop C binding loop residues tends to reflect the strength of the π-cationic interaction.

The distances between the quaternary amine of ACh and the π-cationic contributing residue for ACC-1, ACC-2, and ACC-4 were 4.05 Å, 3.51 Å, and 4.51 Å, respectively (Table 1, Figure 3.12). Additionally, for ACC-1, ACC-2, and ACC-4, the acetyl oxygen of acetylcholine is in fairly close proximity to a polar hydrogen found in the functional group of an Asn (N148:ACC-1, N170:ACC-2, N168:ACC-4) of the complementary subunit's binding loop E (Table 1, Figure 3.12). The major difference between ACC-1 and ACC-2 is noted within loop B, where the residue responsible for contributing to the aromatic box is Phe for ACC-2 (also found in *C. elegans* ACC-1 and ACC-2).

However, for Hco-ACC-1, the analogous residue is shown to be a tyrosine. The polar hydrogen on this Tyr residue is approximately 2.40 Å away from the acetyl oxygen of acetylcholine based on these simulations (Table 1, Figure 3.12).

The interaction of the binding of 3 agonists to ACC-2 were also simulated by docking the molecules to the model of the homodimer for comparison. For example, comparing acetylcholine and carbachol (Table 2, Figure 3.13, A and B), the potential direct interaction is seen with a polar hydrogen from the carbamate group of carbachol and an oxygen of N201 (loop B) which is not seen with acetylcholine.

The distance between the polar hydrogen and the oxygen of N201 was measured as 2.94 Å (Table 2). Additionally, the carbamate group of carbachol is 2.31 Å away from N170 whereas the acetyl oxygen of ACh is 2.77 Å from the same N170 residue (Table 2, Figure 3.12). The π-cationic contributing residue in ACC-2 is W248 of loop C which interacts with the quaternary amine of ligands. ACh appears to have its amine the closest to W248 followed by carbachol then urecholine (Figure 3.13; Table 2).

Interestingly, it appears the proximity of the methyl group present in urecholine (the only difference between urecholine and carbachol) to W248's aromatic ring suggests a change in orientation of the molecule, modifying the distances measured for both the polar hydrogen of the carbamate and the oxygen of N201, as well as the oxygen of the carbamate group and the polar hydrogen of N170 (Table 2, Figure 3.13).

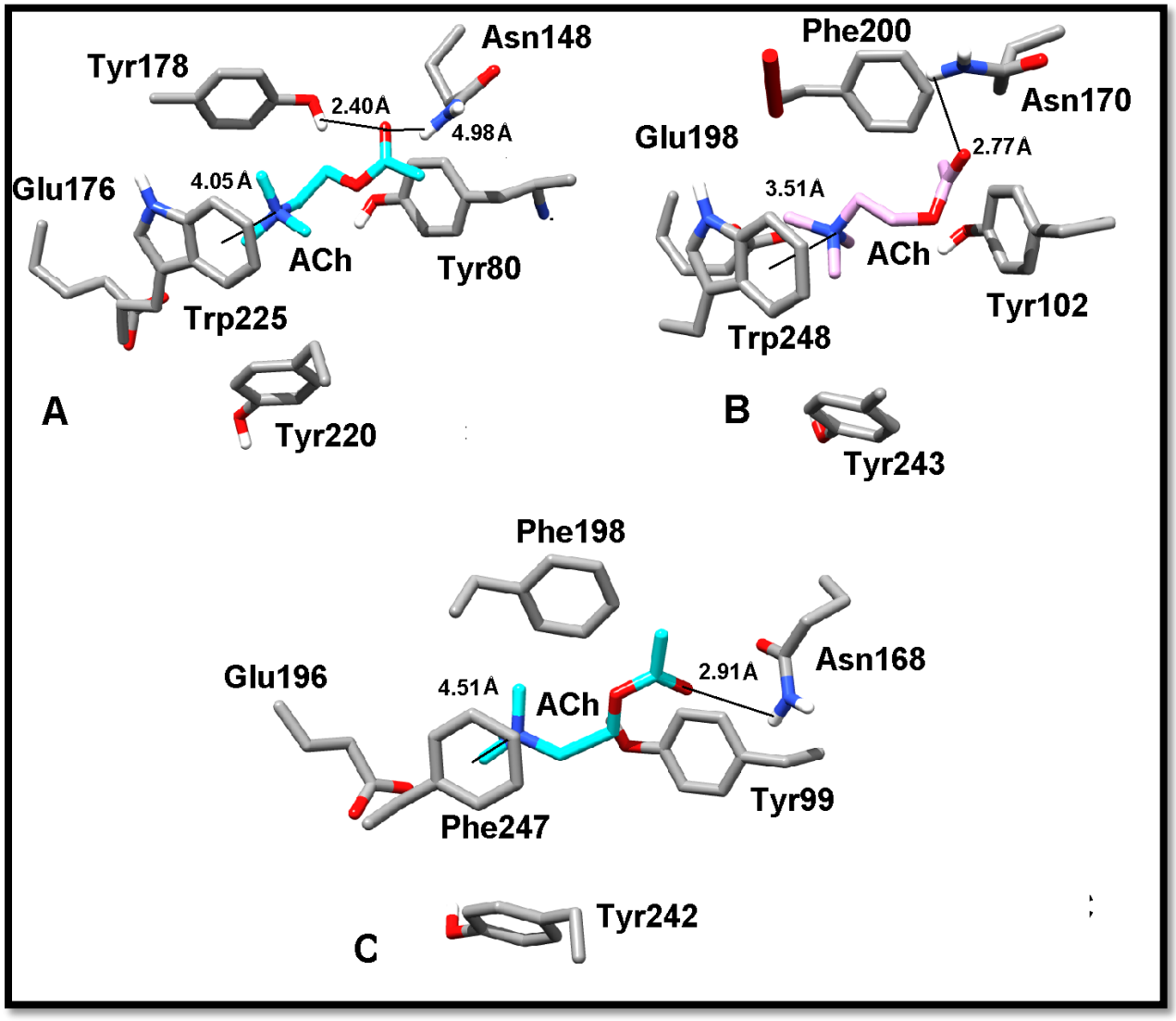

Figure 3.12 - Potential agonist binding site residues of Hco- ACC-1 **(A)**, Hco- ACC-2 **(B)** Hco-ACC-4 **(C)** located within 4.5 Å of all atoms (excluding non-polar hydrogens) of acetylcholine.

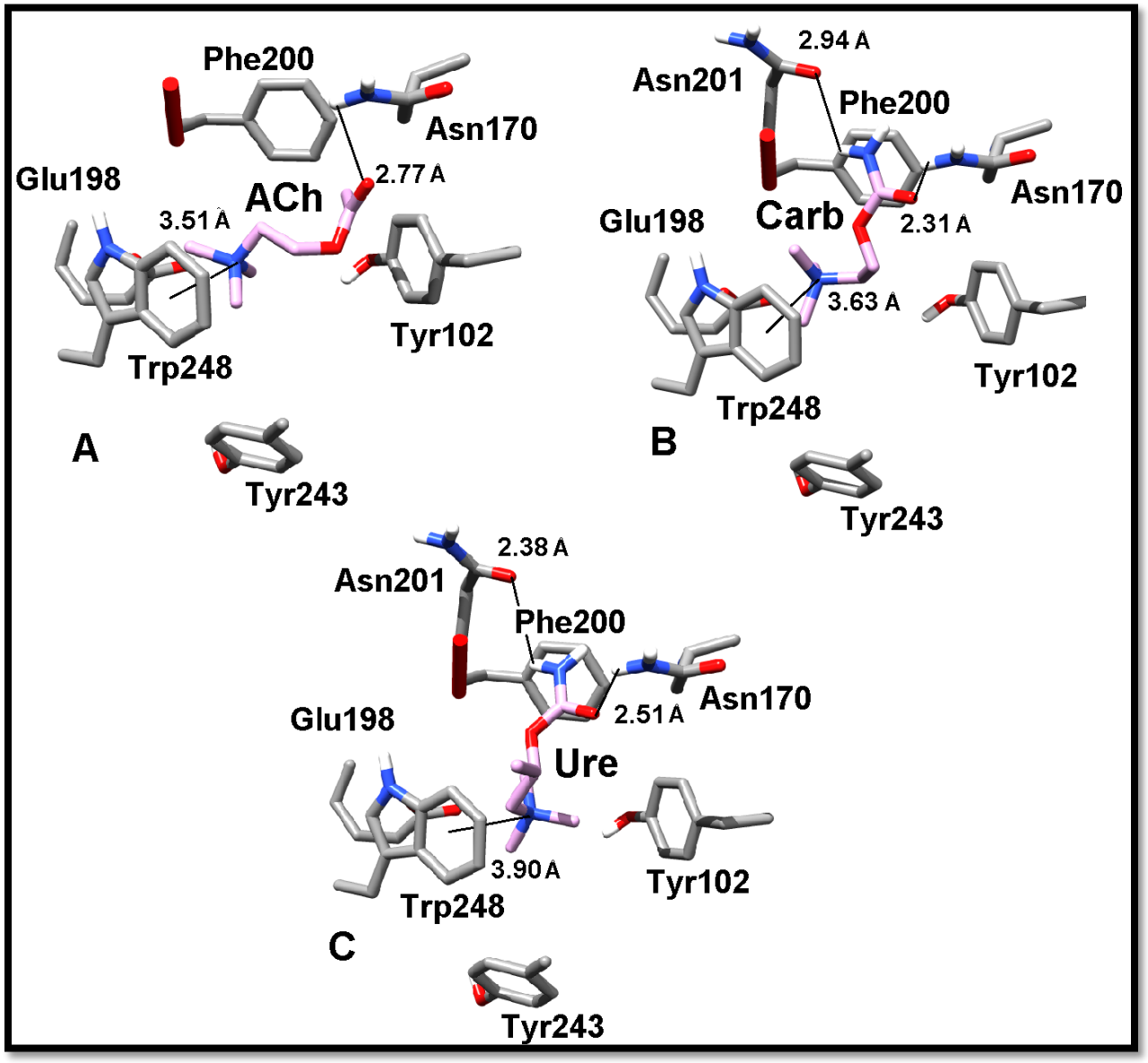

Figure 3.13 - Different agonists docked to the Hco-ACC-2 homodimer. Highest affinity simulations are represented in this figure. The binding affinities were calculated to be -4.6 kcal for ACh, -5.0 kcal for carbachol, and -4.1 kcal for urecholine. **(A)** Hco-ACC-2 homodimer with ACh docked. **(B)** Hco-ACC-2 homodimer with carbachol docked. **(C)** Hco-ACC-2 homodimer with urecholine docked.

Table 1 – Calculated affinities and distances of ACh to the binding site of the homology modelled Hco-ACC-1, Hco-ACC-2, and Hco-ACC-4 dimers. Distance A refers to the distance between the quaternary amine of ACh and the center of benzene from the π-cationic contributing residue. Distance B refers to the distance between analogous Asn residues contributed by binding loop E and the oxygen located on the choline portion of ACh.

Subunit	Affinity to ACh (kcal*mol^{-1})	Distance A (Å)	Distance B (Å)
Hco-ACC-1	**-5.6**	**4.05**	**4.98**
Hco-ACC-2	**-6.3**	**3.51**	**2.77**
Hco-ACC-4	**-4.2**	**4.51**	**2.99**

Table 2 – Calculated affinities and distances of ACh, Carbachol, and Urecholine to the binding site of the Hco-ACC-2 homology modelled dimer. Distance A refers to the distance between the center of the benzene ring located on Trp248 and the quaternary amine of all agonists. Distance B refers to the distance between a polar hydrogen of Asn170 and an oxygen present on all agonists. Distance C refers to the distance between an oxygen of Asn201 and a polar H found on all agonists.

Ligand	Affinity to ACC-2 (kcal*mol^{-1})	Distance A (Å)	Distance B (Å)	Distance C (Å)
Acetylcholine	**-6.3**	**3.51**	**2.77**	**No Polar H**
Carbachol	**-5.8**	**3.63**	**2.31**	**2.94**
Urecholine	**-5.2**	**3.90**	**2.5**	**2.38**

CHAPTER 4: DISCUSSION AND CONCLUSION

This thesis serves to describe the isolation and partial characterization of potentially important anthelmintic target genes *hco-acc-1, hco-acc-2,* and *hco-acc-4.* These are the first members of the ACC family isolated from an important nematode pathogen.

4.1 Characterization of Hco-ACC-1

The sequencing and modelling of Hco-ACC-1 described above has helped to elucidate and further refine the unique structure of the ACC family of chloride channels as compared to nAChRs, in both vertebrates and invertebrates. The presence of the anion selective PAR motif in the M2 domain indicates a vital difference in the fact that vertebrates do not possess anion channels gated by acetylcholine. The most striking difference between Hco-ACC-1 and both alpha and non-alpha nAChRs in terms of ACh binding, is an absence of the signature cys-cys motif in binding loop C.

Secondly, the classical π-cationic interaction seen between the quaternary amine of acetylcholine and a tryptophan residue is still present in the sequence of ACC-1 but is located in loop C rather than in the traditional loop B seen in nicotinic receptors (Beene *et al.* 2002). Interestingly, a similar shifting of this key tryptophan residue from loop B to C is also seen when we compare serotonin 5-HT_3 and nematode MOD-1 receptors (Mu *et al*. 2003).

Recently, Wever *et al*. (2015) provided evidence that the ACC family of receptors were potentially good anthelmintic targets in *C. elegans*. Here, *avr-15* (encoding a GluCl

subunit) under the control of *acc* promoters, exhibited high levels of sensitivity to ivermectin, demonstrating that the ACC family of receptors function in what were referred to as “essential” or anthelmintic sensitive tissues. In this case, one of the essential tissues was extrapharyngeal neurons (Wever *et al.* 2015). Interestingly, while we did not observe the localization of Hco-ACC-1 in any neurons within *H. contortus,* it was consistently localized to pharyngeal muscle tissue.

This result seems to correlate with results seen by Wever *et al.* when examining another subunit from the family, Cel-LGC-49, where localization determined expression pharyngeal muscle of the procorpus. It appears, therefore, that although ACC-1 localizes to different tissues in *H. contortus* compared to *C. elegans,* they both appear to function in tissues that would be considered essential from the point of view of anthelmintic action. The difference in the localization of ACC receptors between *C. elegans* and *H. contortus* resembles the situation observed with the ivermectin target, the GluCl. In *C. elegans,* GluCl subunits localize to pharyngeal muscle (and various neurons) (Dent *et al.* 1997; 2000; Laughton *et al.* 1997), but, in *H. contortus,* the same receptors are exclusively neuronal (Portillo *et al.* 2003). However, both nematodes are still very sensitive to ivermectin with respect to both locomotion and pharyngeal pumping (Dent *et al.* 1997; Wolstenholme 2012). Indeed, the deletion of any *acc* genes in *C. elegans* does cause a slight reduction in pharyngeal pumping rates (Wever *et al.* 2015). It is tempting to speculate that like the GluCls, the ACC family of receptors show different expression patterns but have a similar overall function between *H. contortus* and *C. elegans.* If so, this would further validate that the ACCs are promising drug targets. Further research must be conducted on these subunits, as well as the others found in the ACC-1 family.

4.2 Characterization of Hco-ACC-2

Many of the key details derived from the sequencing and modelling of Hco-ACC-2 are quite similar compared to Hco-ACC-1. The presence of the PAR motif in the M2 region points to Hco-ACC-2 being a chloride channel, which has been previously shown to be the case with Cel-ACC-2 (Putrenko *et al.* 2005). Again, the key π-cationic interaction between acetylcholine and the subunit appears to occur with a loop C Trp, rather than a loop B Trp seen in the nAChRs. Moreover, the structure of binding loop C is significantly different than that of the nAChRs. The signature CC motif in loop C (of the nAChRs) is missing entirely in Hco-ACC-2.

An additional difference noted in ACC-2 between *H. contortus* and *C. elegans* is the sensitivity of the receptors to acetylcholine. It is worth noting that the *C. elegans* ACC-2 appears to be 2-fold more sensitive to acetylcholine (Putrenko *et al.* 2005) compared to the *H. contortus* ACC-2. Similar observations have been observed with orthologues of GluCl and UNC-49 GABA receptor subunits between *C. elegans* and *H. contortus* (McCavera *et al.* 2009; Siddiqui *et al.* 2010). In the case of the UNC-49 receptor, at least one residue in the agonist binding site has been found to be associated with the differences in GABA sensitivity observed between *C. elegans* and *H. contortus* (Accardi and Forrester 2010). While there is much to be learned about the significance of these observations, it is clear that the evolution of nematode parasitism has likely fine-tuned agonist binding for specific functions that are important in parasitic nematodes.

The inclusion of carbachol (carbamoylcholine) in electrophysiological analysis (and modelling) was decided based on its similar structure to acetylcholine, as well as its previous tolerance in vertebrates due to its use in the treatment of glaucoma (Akk and

Auerbach, 1999). The structural difference being the presence of a carbamate group which slightly elongates the molecule and adds 2 polar hydrogens that could interact with nearby polar side chains of residues in the binding pocket which would not normally interact with ACh. This led to the testing of urecholine which is identical to carbachol but with a single methyl group near the quaternary amine. While traditionally characterized as a muscarinic receptor agonist used primarily for the treatment of glaucoma, it was demonstrated here that carbachol could represent an effective agonist of the nematode ACC-2 receptor, achieving a maximal response at 500 µM similar to ACh which was consistently repeated using different batches of oocytes. Carbachol has also been previously shown to be an agonist for muscle nicotinic receptors (Akk and Auerbach, 1999), however the efficacy of carbachol for the nicotinic receptors was much smaller compared to the classical agonist nicotine. For the ACCs nicotine appears to have a much lower efficacy compared to carbachol (Putrenko *et al.* 2005).

In this study, nicotine only produced roughly a 17% maximal response when a 500µM dose was applied to oocytes expressing Hco-ACC-2. Additional research must be done to determine the EC_{50} of carbachol and to determine whether Hco-ACC-2 (and the ACC family in general) responds more robustly to carbachol due to the structural differences between the nAChRs and the ACC receptors. Nevertheless, it is clear that further study of the molecular pharmacology of ACC receptors can provide an excellent opportunity for the study of current AChR agonists and the possible discovery of novel agonists.

4.3 Characterization of Hco-ACC-4

Similarly to Hco-ACC-1 and Hco-ACC-2, Hco-ACC-4 displays the PAR motif suggesting that this subunit contributes to the formation of a pentameric ligand gated ion channel. Additionally, Hco-ACC-4 does not contain the characteristic cys-cys motif

located in binding loop C as seen in the nAChRs. However, Hco-ACC-4 does have an interesting difference compared to Hco-ACC-1 and Hco-ACC-2 in that it does not have a tryptophan residue within either binding loops B or C, but instead it has a phenylalanine residue in each position. This difference is conserved in the Cel-ACC-4 subunit (Putrenko *et al.* 2005), but is not seen in any of the other subunits in the ACC family.

This is quite interesting as the aromatic ring in phenylalanine has the weakest electronegativity, suggesting a much weaker interaction with the positively charged quaternary amine of acetylcholine. In any case it is predicted that ACC-4 cannot bind acetylcholine. This is consistent with the finding Cel-ACC-4 does not form functional homomeric channels but can associate other ACC subunits to form heteromeric channels. (Putrenko *et al.* 2005). In *C. elegans* ACC-4 is required for the function of another ACC family member, LGC-46 (also present in *H. contortus*) which has been localized to presynaptic cholinergic motor neurons (Takayanagi-Kiya *et al.* 2016). It was shown that both loss and gain of function mutations in *cel-lgc-46* affected the release synaptic vesicles in the motor circuit and as such, LGC-46 (and therefore ACC-4) contribute to form heteromeric channels which acts as auto-receptors to maintain tight control of neurotransmitter release (Takayanagi-Kiya *et al.* 2016). It is therefore conceivable that these auto-receptor channels require ACC-4 in order to be less sensitive acetylcholine contributing to their precise overall function.

4.4 Other potentially important residues in ACC-1, 2 and 4

The binding site of the 3 ACCs have a polar residue asparagine located in binding loop E (see Figure 3.12), which aligns with a conserved leucine in the nAChR. Not only is this asparagine found in the ACC family, but also in the cys-loop serotonin (MOD-1),

tyramine (LGC-55), and dopamine (GGR-3 and LGC-53) gated chloride channels. Based on the homology model, it appears that this highly conserved asparagine can potentially form a hydrogen bond with acetylcholine, carbachol and urecholine as shown in the in Hco-ACC-2 model. Due to the degree of conservation of Asn in this location across multiple subunits and channels, which in turn bind different agonists, it likely serves a key role in binding to diverse agonists.

Examination of the binding of ACh, carbachol, and urecholine to Hco-ACC-2, provides interesting information about different potential interactions with other residues within close proximity to the binding site in the ACCs. For example, ACh does not (even in other lower binding energy simulations produced through AutoDock Vina) dock in an orientation where any part of the molecule is within 6 Å to N201 (binding loop B). However, both carbachol and urecholine (which both possess polar hydrogens which are bound to nitrogens within the carbamate) appear to be within 3 Å of the oxygen atom of N201. This information suggests the possibility of a strong hydrogen bond forming with this residue and both carbachol and urecholine which may be responsible for differences seen in binding compared to acetylcholine.

There also exists interesting variability between Hco-ACC-1 and Hco-ACC-2 in terms of the loop B binding site residues. For example, in ACC-1 specifically, there is a tyrosine (Y178) in loop B, whereas for ACC-2 the residue is a phenylalanine (F200). Tyrosine poses a polar hydrogen which appeared to interact with ACh possibly allowing for the formation of an H-bond between it and Y178. Because the polar hydrogen (contributed by the hydroxyl group of Tyr) is not preset in F200, there could be a much

different binding configuration for agonists for ACC-1 compared to ACC-2. This may in turn contribute to a difference in function between these two subunits.

4.5 Conclusion

Evidence presented in this thesis and elsewhere, points to the ACC family as excellent targets for the development of novel anthelmintic agonists. First, this family of receptors is widespread among parasitic nematodes from different clades (Beech *et al.* 2013; Wever *et al.* 2015). Second, they are expressed in tissues that are considered relevant from an anthelmintic point of view (Wever *et al*. 2015; current study). Third, they are not present in mammals (Putrenko *et al.* 2005), and have a novel agonist binding site (current study) which suggests that it could be exploited for the development of a novel drug. Perhaps a further understanding of the key residues important for agonist binding to ACC receptors would be a first step to the eventual discovery of a novel anthelmintic using a rational drug design approach.

In conclusion, this thesis provides the first examination of the role of ACC receptors in parasitic nematodes as well as the structure of a unique acetylcholine binding site. This study also builds on recent research which provided validation of the ACC family as potential anthelmintic targets (Wever *et al*. 2015). While research using *C. elegans* to evaluate anthelmintic targets is an excellent tool to provide relevant information, research on similar targets in parasitic nematodes can provide key information on whether a rational drug design approach might be worthwhile. While there is still much more to be learned about the role of ACC receptors in parasitic nematodes, it is clear that comparing the function of the LGCC family in free-living verses parasitic nematodes can potentially lead to the discovery of future anthelmintic targets and a better understanding of the evolution of parasitism.

REFERENCES

Accardi M, and Forrester S. The *Haemonchus contortus* UNC-49B subunit possesses the residues required for GABA sensitivity in homomeric and heteromeric channels. Mol Biochem Parasitol 2011; 178(1-2):15-22.

Accardi M, Beech R, and Forrester S. Nematode cys-loop GABA receptors: biological function, pharmacology and sites of action for anthelmintics. Invert Neurosci. 2012; 12(1):3-12

Akk G, and Auerbach A. Activation of muscle nicotinic acetylcholine receptor channels by nicotinic and muscarinic agonists. Br J Pharmacol 1999;128(7):1467-76.

Avery L, and Thomas JH. Feeding and Defecation. In: Riddle DL, Blumenthal T, Meyer BJ, et al., editors. *C. elegans* II. 2nd edition. Cold Spring Harbor (NY): Cold Spring Harbor Laboratory Press; 1997. Chapter 24.

Almeida F, Garcia K, *et al.* Multiple resistance to anthelmintics by *Haemonchus contortus* and *Trichostrongylus colubriformis* in sheep in Brazil. Parasitol Int 2010; 59(4): 622-625.

Ashton F, Li J, *et al.* Chemo- and thermosensory neurons: structure and function in animal parasitic nematodes. Vet Parasitol 1999; 84(3-4): 297-316.

Bamber B, Beg A, Twyman R, and Jorgensen E. The *Caenorhabditis elgans* UNC-49 locus encodes multiple subunits of a heteromultimeric GABA receptor. J Neurosci. 1999; 19(13):5348-5359.

Beech R, Callanan M, Rao V, Dawe G, and Forrester S. Characterization of cys-loop receptor genes involved in inhibitory amine neurotransmission in parasitic and free living nematodes. Para Int 2013; 62: 599-605.

Beene D, Price K, Lester H, Dougherty D, and Lummis S. Tyrosine residues that control binding and gating in the 5-hydroxytryptamine 3 receptor revealed by unnatural amino acid mutagenesis. J Neursci. 2004; 24:9097-9104.

Beg A. and Jorgensen E. EXP-1 is an excitatory GABA-gated cation channel. Nat Neurosci 2003; 6(11):1145-1152.

Brejc K, van Dijk W, Klaassen R, Schuurmans M, van Der Oost J, Smit A, and Sixma T. Crystal structure of an ACh-binding protein reveals the ligand-binding domain of nicotinic receptors. Nature. 2001; 411:269-272.

Chao M, Komatsu H, Fukuto H, Dionne H, and Hart A. Feeding status and serotonin rapidly and reversibly modulate a *Caenorhabditis elegans* chemosensory circuit. Proc Natl Acad Sci 2004; 101:15512–15517.

Chitwood B, and Chitwood M. Anatomy. In *An Introduction to Nematology.* C. Chitwood, ed. 1950. (Monumental Publ. Co., Baltimore).

Coyne M, and Smith G. The mortality and fecundity of *Haemonchus contortus* in parasite-naive and parasite-exposed sheep following single experimental infections Int J Parasitol 2006;22(3): 315-325.

Cully D, Vassilatis D, Liu K, Paress P, Van der Ploeg L, Schaeffer J, and Arena J. Cloning of an avermectin-sensistive glutamate-gated chloride channel from *Caenorhabditis elegans.* Nature. 1994; 371(6499):707-711.

Davis R, and Stretton A. Extracellular recordings from the motor nervous system of the nematode *Ascaris suum.* J. Comp. Phys. 171:17-28.

Dent J, Davis M, and Avery L. *Avr-15* encodes a chloride channel subunit that mediates inhibitory glutamatergic neurotransmission and ivermectin sensitivity in *Caenorhabditis elegans.* EMBO J 1997; 16(19):5867–5879.

Dent J, Smith M, Vassilatis D, and Avery L. The genetics of ivermectin resistance in *Caenorhabditis elegans*. Proc Natl Acad Sci 2009; 97(6): 267-2679.

Dougherty D. Cys-loop neuroreceptors: structure to the rescue? Chem Rev 2008; 108:1642-1653.

Frohman M, Dush M, and Martin G. Rapid production of full-length cDNAs from rare transcripts: amplification using a single gene-specific oligonucleotide primer. Proc Natl Acad Sci 1994; 85:8998–9002.

Geary T, Sims S, Thomas E, Vanover L, Davis P, Winterrowd C, Klein R, Ho N, and Thompson D. *Haemonchus contortus*: ivermectin-induced paralysis of the pharynx. Exp Parasitol 1993; 77(1): 88-96.

Harel M, Kasher R, Nicholas A, Guss J, Balass M, Fridkin M, and Fuchs S. The binding site of acetylcholine receptor as visualized in the X-ray structure of a complex between alpha-bungarotoxin and a mimotope peptide. Neuron 2001; 32(2): 265-275.

Harris J, and Crofton H. Structure and function in the nematodes: internal pressure and cuticular structure in *ascaris.* J Exp Bio 1957; 34:116-130.

Hibbs R, and Gouaux E. Principles of activation and permeation in an anion-selective Cys-loop receptor. Nature 2011; 474(7349):54-60

Hoberg E, Lichtenfels J, *et al.* Phylogeny for species of *Haemonchus* (Nematoda: Trichostrongyloidea): considerations of their evolutionary history and global biogeography among *Camelidae* and *Pecora* (Artiodactyla). J Parasitol 2004; 90(5): 1085-1102.

Hobert O. PCR fusion-based approach to create reporter gene constructs for expression analysis in transgenic *C. elegans*. Biotechniques 2002; 32:728-30.

Irwin J, Sterling T, Mysinger MM, Bolstad ES and Coleman RG. ZINC: a free tool to discover chemistry for biology. J Chem Inf Model 2002; 23; 52(7):1757-68.

Jensen M, Pedersen L, Timmermann D, Schousboe A, and Ahring P. Mutational studies using a cation-conducting GABAA receptor reveal the selectivity determinants of the cys-loop family of ligand-gated ion channels. J Neurochem 2005; 92(4):962-72.

Jones A, and Sattellle D. The cys-loop ligand-gated ion channel gene superfamily of the nematode, *Caenorhabditis elegans*. Invert Neurosci 2008; 8(1):41-47.

Kaji M, Kwaka A, Callanan M, Nusrat H, Desaulaniers J, and Forrester S. A molecular characterization of the agonist binding site of a nematode cys-loop GABA receptor. Br J Pharmacol. 2015; 172(15):3737-3747.

Kaminsky R, Gauvry N, Schorderet-Weber S, Skripsky T, Bouvier J, Wenger A, Schroeder F, Desaules Y, Hotz R, Goebel T, Hosking B, Pautrat F, Wieland-Berghausen S, and Ducray P. Identification of the amino-acetonitrile derivative monepantel (AAD1566) as a new anthelmintic drug development candidate. Parasitol Res 2008; 103(4): 931-939.

Kelley L, *et al.* The PHYRE2 web-portal for protein modelling, prediction and analysis. Nature Proc 2015; 10:845-858.

Köhler P. The biochemical basis of anthelmintic action and resistance. Int J Parasitol 2001; 31(4): 336–345.

Laing R, Kikuchi T, Martinelli A, Tsai I, Beech R, *et al.* The genome and transcriptome of *Haemonchus contortus*, a key model parasite for drug and vaccine discovery. Gen Biol 2013; 14(8), R88

Laskowski R, MacArthur M, Moss D, and Thornton J. PROCHECK - a program to check the stereochemical quality of protein structures. J App Cryst 1993; 26: 283-291.

Laughton D, Lunt G, and Wolstenholme A. Alternative splicing of a *Caenorhabditis elegans* gene produces two novel inhibitory amino acid receptor subunits with identical ligand binding domains but different ion channels. Gene 1997; 201:119-125.

Lummis S, Beene D, Harrison N, Lester H, and Dougherty D. A cation-pi binding interaction with a tyrosine in the binding site of the GABAC receptor. Chem Biol 2005; 12:993-997.

McCavera S, Rogers AT, Yates DM, Woods DJ, and Wolstenholme AJ. An ivermectin-sensitive glutamate-gated chloride channel from the parasitic nematode *Haemonchus contortus*. Mol Pharmacol 2009; 75(6):1347-55.

Mehlhorn H. (2008) Encyclopedia of Parasitology (3rd edn). Springer, Berlin Heidelberg.

Mello C, and Fire A. DNA Transformation. Methods Cell Biol 1995; 48: 451-82.

Morris GM, Huey R, Lindstrom W, Sanner MF, Belew RK, Goodsell DS, *et al*. AutoDock4 and AutoDockTools4: Automated docking with selective receptor flexibility. J Comput Chem 2009; 30(16):2785-91.

Mu T, Lester H, and Dougherty D. Different binding orientation for the same agonist at homologous receptors: a lock and key or a simple wedge? J Am Chem Soc 2003; 125:6850-6851.

Nikolaou S, and Gasser R. Prospects for exploring molecular developmental processes in *Haemonchus contortus*. Int J Parasitol 2003; 36(8): 859-868.

Padgett C, Hanek P, Lester H, Dougherty D, and Lummis S. Unnatural amino acid mutagenesis of the GABAA receptor binding site residues reveals a novel cation-pi interaction between GABAB and beta 2Tyr97. J Neurosci 2007; 27:886-892.

Pereira L, Kratsios P, Serrano-Saiz E, Sheftel H, Hobert O, *et al.* A cellular and regulatory map of the cholinergic nervous system of *C. elegans*. Elife 2015. pii: e12432. doi: 10.7554/eLife.12432.

Pirri J, McPherson A, Donnelly J, Francis M, and Alkema M. A tyramine-gated chloride channel coordinates distinct motor programs of a *Caenorhabditis elegans* escape response. Neuron. 2009; 62(4):526-538.

Pettersen EF, Goddard TD, Huang CC, Couch GS, Greenblatt DM, Meng EC, *et al*. UCSF Chimera--a visualization system for exploratory research and analysis. J Comput Chem 2004; 25(13):1605-12.

Pless S, Millen K, Hanek A, Lynch J, Lester H, Lummis S, and Dougherty D. A cation-pi interaction in the binding site of the glycine receptor is mediatied by a phenylalanine residue. J Neruosci 2008; 28:10937-10942.

Portillo V, Jagannathan S, and Wolstenholme A. Distribution of glutamate-gated chloride channel subunits in the parasitic nematode *Haemonchus contortus*. J Comp Neurol 2003; 462(2):213-222.

Putrenko I, Zakikhani M, *et al*. A family of acetylcholine-gated chloride channel subunits in *Caenorhabditis elegans*. J Biol Chem 2005;280(8): 6392-6398.

Rao V, Siddiqui S, Prichard R, and Forrester S. A dopamine-gated ion channel (HcGGR3*) from *Haemonchus contortus* is expressed in the cervical papillae and is associated with macrocyclic lactone resistance. Mol Biochem Parasitol 2009; 166(1):54-61.

Ranganathan R, Cannon S, and Horvitz H. Mod-1 is a serotonin-gated chloride channel that modulates locomotory behavior in *C. elegans.* Nature. 408(6811):470-475.

Raza A, Lamb J, Chambers M, Hunt P, and Kotze A. Larval development assay reveal the presence of sub-populations showing high- and low-level resistance in a monepantel (Zolvix®)-resistant isolate of *Haemonchus contortus*. Vet Parasitol 2016; 220:77-82.

Reger J. The fine structure of fibrillar components in plasma membrane contacts in esophageal myoepithelium of *Ascairs lumbricoides* (var. *suum).* J Ultrastruct Res 1966; 14:602-617.

Ringstad N, and Abe, N. Ligand-gated chloride channels are receptors for biogenic amines in C. elegans. Science 2009; 325(5936):96-100.

Saeed M, Iqbal Z, *et al*. Multiple anthelmintic resistance and the possible contributory factors in Beetal goats in an irrigated area (Pakistan). Res Vet Sci 2010; 88(2): 267-272.

Sali A, and Blundell T. Comparative protein modeling by satisfaction of special restraints. J Mol Biol 1993; 243(3):779-815.

Sarai R, Kopp S, Knox M, Coleman G, and Kotze A. *In vitro* levamisole selection pressure on larval stages of *Haemonchus contortus* over nine generations gives rise to drug resistance and target site gene expression changes specific to the early larval stages only. Vet Parasitol 2015; 211(1-2):45-53.

Siddiqui S, Brown D, Rao V, and Forrester S. An UNC-49 GABA receptor subunit from the parasitic nematode *Haemonchus contortus* is associated with enhanced GABA sensitivity in nematode heteromeric channels. J Neurochem 2010; 113(5):1113-22.

Sievers F, Wilm A, Dineen D, Gibson T, Lopez R, Thompson J, and Higgins D. Fast, scalable generation of high-quality protein multiple sequence alignments using Clustal Omega. Mol Sys Bio 2015; 7: 539.

Sine S, and Engel A. Recent advances in cys-loop receptor structure and function. Nature 440(7083): 2006; 448-455.

Stretton A. Anatomy and development of the somatic musculature of the nematode *Ascaris.* J Exp Biol 1976; 64:773-788.

Takayanagi-Kiya S, Zhou K, and Jin Y. Release-dependent feedback inhibition by a presynaptically localized ligand-gated anion channel. *eLife*. 2016;5:e21734. doi:10.7554/eLife.21734.

Thompson N, Navaratnarajah P, and Wang X. Measuring surface binding thermodynamics and kinetics by using total internal reflection with fluorescence correlation spectroscopy: practical considerations. J Phys Chem B 2010; 13; 115(1):120-131.

Trott O, Olson A. AutoDock Vina: improving the speed and accuracy of docking with a new scoring function, efficient optimization, and multithreading. J Comput Chem 2010; 30; 31(2):455-61.

Tyrrell K, and LeJambre L. Overcoming macrocyclic lactone resistance in Haemonchus contortus with pulse dosing of levamisole. Vet Parasitol 2010; 168(3-4): 278-283.

Urdaneta-Marquez L, Bae S, Janukavicius P, Beech R, Dent J, and Prichard R. A dyf-7 haplotype causes sensory neuron defects and is associated with macrocyclic lactone resistance worldwide in the nematode parasite *Haemonchus contortus*. Int J Parasitol 2014; 44(14):1063-71.

Van Doren K, and Hirsh D. Trans-spliced leader RNA exists as small nuclear ribonucleoprotein particles in *Caenorhabditis elegans*. Nature 1988; 6; 335(6190):556-9.

Weston D, Patel B, and Van Voorhis W. Virulence in *Trypanosoma cruzi* infection correlates with the expression of a distinct family of sialidase superfamily genes. Mol Biochem Parasit 1999; 98:105–116.

Wever C, Farrington D, and Dent J. The Validation of Nematode-Specific Acetylcholine-Gated Chloride Channels as Potential Anthelmintic Drug Targets. PLoS One. 2015; 2210(9).

Wolstenholme A. Glutamate-gated chloride channels. J Bio Chem. 2012; 287(48):40232-40238

White J. The Anatomy. In The Anatomy of *Caenorhabditis elegans.* W.B. Wood, ed. Cold Springs Harbour Laboratory, New York. 81-122.

Zhang J, Xue F, Chang Y. Structural determinants for antagonist pharmacology that distinguish the rho1 GABAC receptor from GABAA receptors. Mol Pharmacol 2008; 74(4):941-51.

Zhong W, Gallivan J, Zhang Y, Li L, Lester H, and Dougherty D. From ab initio quantum mechanics to molecular neurobiology: a cation-pi binding site in the nicotinic receptor. Proc Natl Acad Sci 1998; 95:12088-12093.